JAERI-Tech
2003-084

QUANTITATIVE EXPERIMENTS ON THERMAL HYDRAULIC CHARACTERISTICS OF AN ANNULAR TUBE WITH TWISTED FINS

November 2003

Koichiro EZATO, Masayuki DAIRAKU, Masaki TANIGUCHI
Kazuyoshi SATO, Satoshi SUZUKI and Masato AKIBA

日本原子力研究所
Japan Atomic Energy Research Institute

本レポートは，日本原子力研究所が不定期に公刊している研究報告書です。
入手の問合わせは，日本原子力研究所研究情報部研究情報課（〒319-1195　茨城県那珂郡東海村）あて，お申し越しください。なお，このほかに財団法人原子力弘済会資料センター（〒319-1195　茨城県那珂郡東海村日本原子力研究所内）で複写による実費頒布をおこなっております。

This report is issued irregularly.
Inquiries about availability of the reports should be addressed to Research Information Division, Department of Intellectual Resources, Japan Atomic Energy Research Institute, Tokai-mura, Naka-gun, Ibaraki-ken, 319-1195, Japan.

編集兼発行　　日本原子力研究所

JAERI-Tech 2003-084

Quantitative Experiments on Thermal Hydraulic Characteristics of an Annular Tube with Twisted Fins

Koichiro EZATO, Masayuki DAIRAKU, Masaki TANIGUCHI,
Kazuyoshi SATO, Satoshi SUZUKI and Masato AKIBA

Department of Fusion Engineering Research
Naka Fusion Research Establishment
Japan Atomic Energy Research Institute
Naka-machi, Naka-gun, Ibaraki-ken

(Received September 10, 2003)

Thermal hydraulic experiments measuring critical heat flux (CHF) and pressure drop of an annular tube with twisted fins, "annular swirl tube", has been performed to examine its applicability to the ITER divertor cooling structure. The annular swirl tube consists of two concentric circular tubes, the outer and inner tubes. The outer tube with outer and inner diameters (OD and ID) of 21 mm and 15 mm is made of Cu-alloy that is CuCrZr and one of candidate materials of the ITER divertor cooling tube. The inner tube with OD of 11 mm and ID of 9 mm is made of stainless steal. It has an external swirl fin with twist ratio (y) of three to enhance its heat transfer performance. In this tube, cooling water flows inside of the inner tube first, and then returns into an annulus between the outer and inner tubes with a swirl flow at an end-return of the cooling tube.

The CHF experiments show that no degradation of CHF of the annular swirl tube in comparison with the conventional swirl tube whose dimensions are similar to those of the outer tube of the annular swirl tube. A minimum axial velocity of 7.1 m/s is required to remove the incident heat flux of 28MW/m^2, the ITER design value. Applicability of the JAERI's correlation for the heat transfer to the annular swirl tube is also demonstrated by comparing the experimental results with those of the numerical analyses.

The friction factor correlation for the annular flow with the twisted fins is also proposed for the hydrodynamic design of the ITER vertical target. The least pressure drop at the end-return is obtained by using the hemispherical end-plug. Its radius is the same as that of ID of the outer cooling tube.

These results show that thermal-hydraulic performance of the annular swirl tube is promising in application to the cooling structure for the ITER vertical target.

Keywords: ITER, Divertor, Annular Swirl Tube, Critical Heat Flux, Heat Transfer, Pressure Drop, End-return

JAERI-Tech 2003-084

ねじりフィン付き同軸2重管の熱流動実験

日本原子力研究所那珂研究所核融合工学部
江里 幸一郎・大楽 正幸・谷口 正樹・佐藤 和義・鈴木 哲・秋場 真人

(2003年 9月 10日受理)

ITER ダイバータの冷却構造への適用性を検討するために、ねじりフィン付き同軸 2 重管(同軸スワール管)の限界熱流束及び圧力損失の測定実験を行った。本同軸 2 重管は外管および内管から構成される。外管形状は外径 21mm、内径 15mm の円管であり、材質は ITER ダイバータ冷却管の候補材料である銅合金(CuCrZr)である。内管形状は外径 11mm、内径 9mm であり、ステンレス製である。内管の外表面には、熱伝達特性を向上させるため、ねじり比 3 のねじりフィンが加工してある。本冷却管において、冷却水は内管に先ず供給され、端部のエンドプラグで外管と内管間の環状流路へ、旋回流として折り返し流れる。

限界熱流束測定実験の結果、本ねじりフィン付き同軸2重管の限界熱流束は、同じ外径寸法のスワール管と同等の表面限界熱流束を有することが確認できた。このとき、ITER ダイバータ冷却に必要な表面限界熱流束、28MW/m^2 を得るのに必要な冷却水の最小軸流速は 7.1m/sec であった。また、実験値と数値解析の結果を比較することにより、原研が開発したスワール管の熱伝達係数の相関式がねじりフィン付き同軸管に適用可能であることを示した。

端部の折返し部の圧力損失は、外管内径と同じ半径を有する半球状のエンドプラグで最小となることが確認され、ITER ダイバータの冷却系設計に必要な環状流路部の圧力損失および管摩擦係数を評価した。

これらの結果により、ねじりフィン付き同軸流路は ITER ダイバータ垂直ターゲットへ適用するのに十分な熱流動特性を有することを明らかにした。

那珂研究所：〒311-0193 茨城県那珂郡那珂町向山 801-1

Contents

目　次

1. Introduction

The vertical target of the ITER divertor has to be designed for high heat fluxes up to 20 MW/m^2 for 10 s. In the reference design of the ITER divertor, CFC monoblocks with a swirl cooling tube and pressurized water flow are adopted to handle such high heat flux conditions. In this design, abundance of small tubes and space at the lower end of the vertical target are required for the water manifold with a complicated geometry [1]. To eliminate these requirements and to develop the alternative concept for the vertical target cooling system, an annular flow concept of the CFC monoblock with concentric feed and return is proposed. Within this concept the coolant feed and return is located at one end of the vertical target as shown in Fig. 1-1.

The annular cooling tube consists of two concentric tubes, an outer tube and an inner tube. The outer tube is brazed to the CFC monoblock armour tiles. The inner tube has external twisted fins to enhance heat transfer. In this cooling tube, ì annular swirl tubeî, coolant flows inside the inner tube first and then returns via the annulus between the outer and inner tubes with a swirl flow. However, experimental data on the annular swirl flow such pressure drop and critical heat flux (CHF) under ITER-relevant conditions have not been reported enough comparing with the other cooling structures [2], which are indispensable to design the components with the annular flow concept.

In the present study, thermal-hydraulic characteristics of the annular swirl tube are investigated in order to compare with those of the conventional swirl tube. For this purpose, two kinds of experiments using the annular swirl tube are carried out: one is pressure drop experiment on the annular section and the end-return of the cooling tube. At the end-return, the water flow changes its direction 180 degrees and large pressure drop is expected. Therefore, we provided several shapes of the end-return geometry and experiments were carried out to minimize the pressure drop at the end-return. As a result, experimental correlation to predict the pressure drop of the annular swirl tube is proposed. The other is heating experiments on the annular swirl tube to investigate the heat removal characteristics and CHF limit under ITER-relevant one-sided heating condition. These results are compared with the existing correlations for heat transfer coefficients and CHF to examine their applicability to the annular swirl tube.

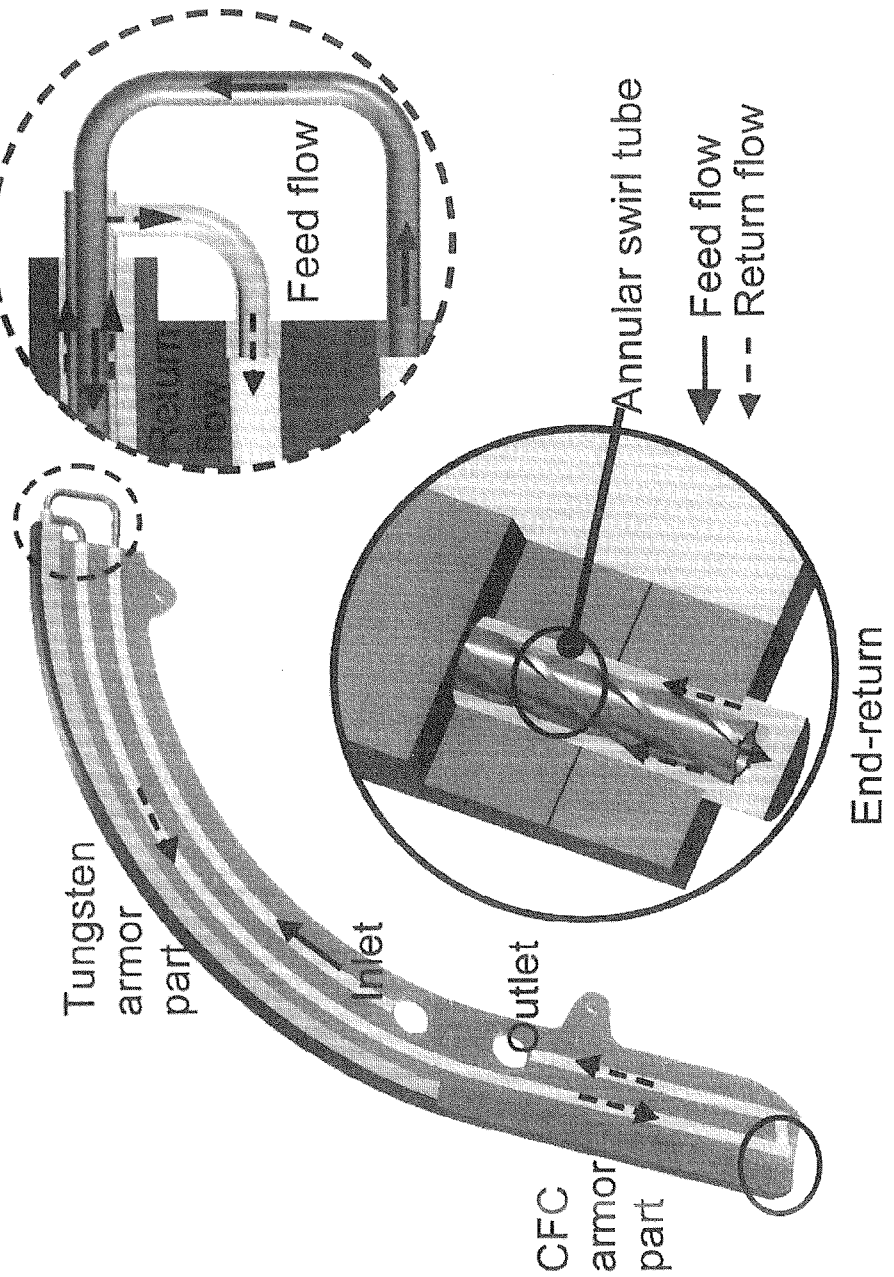

Figure 1-1 Concept of vertical target with an annular flow concept.

2. Experiments

2.1. Experimental facility

Experiments have been carried out using the Particle Beam Engineering Facility (PBEF) in JAERI. PBEF can generate the intense hydrogen ion beams up to 1.5 MW for durations for 0.01 to 1000 sec. It consists of a vacuum chamber, an ion source, a high voltage power supply system, a test bed, a cooling water system, a vacuum pumping system, a control system, and a data acquisition system as shown in Fig. 2-1. The vacuum chamber has many installation ports for measuring equipments and data acquisition systems. Major dimensions of the vacuum chamber are 4 m in height, 3.5 m in width and 7 m in length. The ion source is mounted as a heat source at the top of the vacuum chamber and consists of a source plasma generator and an acceleration grid system. At the source plasma generator, hydrogen source plasma is produced by arc discharge process using tungsten filaments. Only hydrogen ions are stably extracted by the acceleration grid system at beam energies raging from 16 to 50 keV with the beam current up to 30A.

In the present experiment, a test sample is set into the vacuum chamber as shown in Fig. 2-1 to form a horizontal flow. The center of the test sample corresponded to the center of the ion beam. At the bottom of the test bed, an actively cooled ion dump is installed to handle the intense ion beam at steady state because an area of the intense ion beams is much wider than the test sample. It consists of an array of copper swirl and smooth tubes with an external fin. The water-cooling system consists of de-ionized water-cooling loops and a heat exchanger loop. Circulating conditions of the cooling water for the test section are as follows: pressure up to 2.0 MPa; flow rate up to 3000 ℓ/min; and, inlet temperature of the test sample from 25 to 35 °C. On the top of the test bed, a movable multichannel calorimeter is used to measure magnitude of the incident heat flux and its profile. The heated surface of the test sample is observed with two charge-coupled device (CCD) color cameras and an Infrared (IR) camera, and a two-color pyrometer located at the top and upper part of the vacuum chamber. The data acquisition system with the sampling speed of 10 Hz is used to record the various signals from thermocouples, flow meter, pressure gages and beam operation system such as acceleration voltage and current during the experiment.

2.2. Test samples

Detailed specifications of the annular swirl tube are shown in Fig. 2-2. The annular swirl tube consists of two concentric tubes; an outer tube made of CuCrZr and an inner tube made of stainless steel. In this test sample, the water flows into the inside of the inner tube at first; at an end-return, a nozzle distributes the water into the annular gap between the outer and inner tubes. The water returns in the annular gap to the outlet of the tube with a swirl flow. Dimensions of the outer tube are 21mm in outside diameter (OD) and 15mm in inside diameter (ID), and those of the inner tube are 11mm OD and 9 mm ID. The inner tube has twisted fins on its external surface to enhance heat transfer characteristics. The twist ratio (y) defined as a ratio of pitch of 180° rotation of the fin to ID of the outer tube is three as shown in Fig. 2-3. The twisted fins are made with direct milling from a thick SS tube. Pressure taps at the inlet and outlet sections of the mock-up are used for the pressure drop experiment. To measure the outer tube wall temperature, three K-type sheathed thermocouples with an outer diameter of 0.5 mm are brazed into the tube material at the center with an interval of 10mm. Each thermocouple is located 0.2 mm below the heated surface and is installed into the material from the rear part of the test section. As shown in Fig. 2-4, six different types of plugs for the end-return are prepared to find the suitable shape of the end-return providing the least pressure drop.

Thermal performance of the present annular swirl tube is compared with that of a conventional swirl tube with a twisted tape experimentally. Its tube dimensions are similar to those of the outer tube of the annular swirl tube, that is, 21 mm in OD and 15 mm in ID. The twist ratio (y) of the swirl tape to the inner diameter is three and its thickness is 0.2 mm.

2.3. Experimental procedure

For each test, thermal hydraulic conditions (i.e., pressure at the middle of the test sample and inlet volumetric flow rate) and parameters that control the ion beam (mainly, pulse duration, acceleration voltage and current) are selected. Pressure and volumetric flow rate are adjusted by means of inlet and outlet valves by remote control. The cooling water conditions are as follows; local pressures at the center of test sample are

raging from 0.96 to 1.06 MPa. The volumetric flow rates are varied from 11.0 to 65.5 l/min. The inlet temperatures are set from 26 to 33 °C. The pulse durations are chosen to make the test sample reach the thermally steady state condition. It is judged by the wall temperature data measured with the thermocouples. The incident heat fluxes to the surface of the test sample are measured with the movable multichannel calorimeter and also the cross-check of those values is performed by water calorimeter calculation after experiments as mentioned detailed later.

Prior to the heating experiments, pressure drop of the annular swirl tube is measured at ambient temperature. First, the pressure drops in the inner smooth and outer annular tubes are measured separately by using an extension tube instead of the end-return. Then pressure drop at the end-return is estimated by subtracting the estimated pressure drops at the other section of the test sample from the measured total pressure drop of the test sample. The pressure drops in the other sections including the inlet and outlet tubes are calculated by using the existing correlations of friction factor and pressure drop for the smooth and annular tube. Details of the correlations are described in the following subsection, 2.4.

In the CHF testing, the flow rate of the cooling water is decreased step by step to reach burnout under the fixed heat flux condition. The burnout phenomenon is detected by means of the thermocouples inserted into the outer tube material and the IR camera, that is, after reaching steady-state temperature, temperature excursion is detected with either the thermocouples or the IR camera when the burnout phenomenon occurred. The ion beam is stopped by a safety trigger connecting the thermocouples or by the occurrence of the temperature excursion on the tube surface in order to avoid melting of the tube material. The trigger value set from 500 to 600 °C is effective to catch the burnout and to prevent the test sample from water leakage.

2.4. Pressure drop correlation for data analyses

Pressure drop in each section of the annular swirl tube is measured at first, that is, the inner smooth and outer swirl annulus tubes. Then the pressure drop at the end-return is estimated by subtracting the pressure drop estimated at the other section of the mock-up from the experimental results. The pressure drops in the other sections including the inlet and outlet tubes are calculated by following correlations.

The pressure drop caused by friction loss in the inner smooth tube section is calculated by the following Darcy-Weisbach equation,

$$\Delta P = \frac{1}{2}\lambda \frac{L}{D_H}\rho U_{ax}^2, \tag{2-1}$$

where, ΔP is the pressure drop in a length L of the pipe, D_H is the hydraulic diameter of tube, ρ is the density of water, and U_{ax} is the average axial velocity. The friction factor λ is given by

$$\lambda = 0.3164 \mathrm{Re}_H^{-0.25} \quad \text{for} \quad 2000 < \mathrm{Re_H} < 10^5, \tag{2-2}$$

$$\lambda = 0.0032 + 0.221 \mathrm{Re}_H^{-0.237} \quad \text{for} \quad \mathrm{Re_H} > 10^5, \tag{2-3}$$

where, Re_H is Reynolds number based on D_H and U_{ax}.

The pressure drop at an abrupt expansion of the flow path is given by

$$\Delta P = \zeta \frac{1}{2}\rho U_1^2, \qquad \zeta = \xi(1 - A_1/A_2)^2, \tag{2-4}$$

where, U_1 is the average axial flow velocity before the abrupt expansion, A_1 and A_2 are cross-sectional areas before and after the abrupt expansion, ξ is the loss coefficient for the abrupt expansion and shows unity in the present study.

The pressure drop at an abrupt contraction of flow path is given by

$$\Delta P = \zeta \frac{1}{2}\rho U_2^2, \qquad \zeta = (A_2/A_c - 1)^2, \tag{2-5}$$

where, U_2 is the axial flow velocity after the abrupt contraction of flow path, A_2 and A_c are cross-sectional areas before and after the abrupt contraction, ξ is the contraction factor given by Table 2-1.

Table 2-1 loss factor at an abrupt contraction of flow path

A_2/A_1	0.1	0.2	0.3	0.4	0.5	0.6	0.7	0.8	0.9	1.0
A_c/A_2	0.61	0.62	0.63	0.65	0.67	0.70	0.73	0.77	0.84	1.0
ζ	0.41	0.38	0.34	0.29	0.24	0.18	0.14	0.089	0.036	0.0

The pressure drop in the annular tube section with the twisted fins is calculated by

$$\Delta P = \frac{1}{2}\lambda \frac{L_{sw}}{D_H}\rho U_{sw}{}^2, \tag{2-6}$$

where, U_{sw} is the average swirl flow velocity of the coolant. The relationship between the swirl flow velocity, U_{sw} and axial flow velocity, U_{ax} is

$$U_{sw} = U_{ax}\sqrt{1+\pi^2/4T_R^2}\,. \tag{2-7}$$

The corrected length of the flow path with the twisted fins, L_{sw}, is expressed as

$$L_{sw} = L\sqrt{1+\pi^2/4T_R^2}\,, \tag{2-8}$$

where, T_R is defined as the twist ratio (y) of the inner diameter of the outside tube and a 180° rotation of the twisted fins (= 3).

The friction factor has been obtained from the pressure drop experiments performed by CEA on the mock-up of annular flow called AF1 [3, 4]; the local friction factor λ can be expressed by

$$\lambda = 0.225\mathrm{Re}_{H,sw}^{-0.2053}, \tag{2-9}$$

where $\mathrm{Re}_{H,sw}$ is Reynolds number based on D_H and U_{sw}, is expressed by

$$\mathrm{Re}_{H,sw} = \rho D_H U_{sw}/\mu\,. \tag{2-10}$$

2.5. Measurement of heat flux profile

The incident heat flux and its profile are measured with the multichannel calorimeter located on the test bed. The multichannel calorimeter consisted of two dimensional array of small copper chips which have a surface area S = 2.7 cm^2 and a volume v = 1.4 cm^3 as shown in Fig. 2-5. A thermocouple is bonded on the rear side of each copper chip to measure its temperature in adiabatic condition. To minimize heat conduction loss from the chip, we supported each copper chip adiabatically by using a stainless steal bolt. The incident heat flux is calculated from the temperature rise of the copper chip using the following equation,

$$q = \frac{v}{S}\rho C_p \frac{\Delta T_2 - \Delta T_1}{\tau_2 - \tau_1}, \tag{2-11}$$

where, q, ρ and C_p are the incident heat flux, density and specific heat of copper, respectively. Moreover, ΔT_1 and ΔT_2 are the temperature rises during the ion beam irradiation with the durations of τ_1 and τ_2. In the present study, τ_1 and τ_2 are set to 40 and 80 ms.

Figure 2-6 shows the typical incident heat flux profiles as a function of position of the test sample under different acceleration voltages (Vacc) and ion beam currents (Iacc) conditions. These profiles show almost Gaussian profiles in the direction parallel to a water flow.

Comparison of the experimental temperature rise of the cooling water in the test sample with calorimetric calculation at the experimental heat flux condition is shown in Fig. 2-7 to check the results of the heat flux measurements. In this figure, a horizontal axis represents the temperature rise of the cooling water measured by the thermocouples located at the inlet and outlet of the test sample. A vertical axis represents those of calorimetric calculation based on the measured heat flux profile in the flow direction. In this calculation, we assume that the heat flux distribution crosswise the flow direction is flat because changes of the heat flux profiles are very small within the width of the test sample (= 21 mm) as shown in Fig. 2-6. The experimental and calculated results are in good agreement with a difference within ± 10% difference for all heat flux profiles which are applied to the CHF testing.

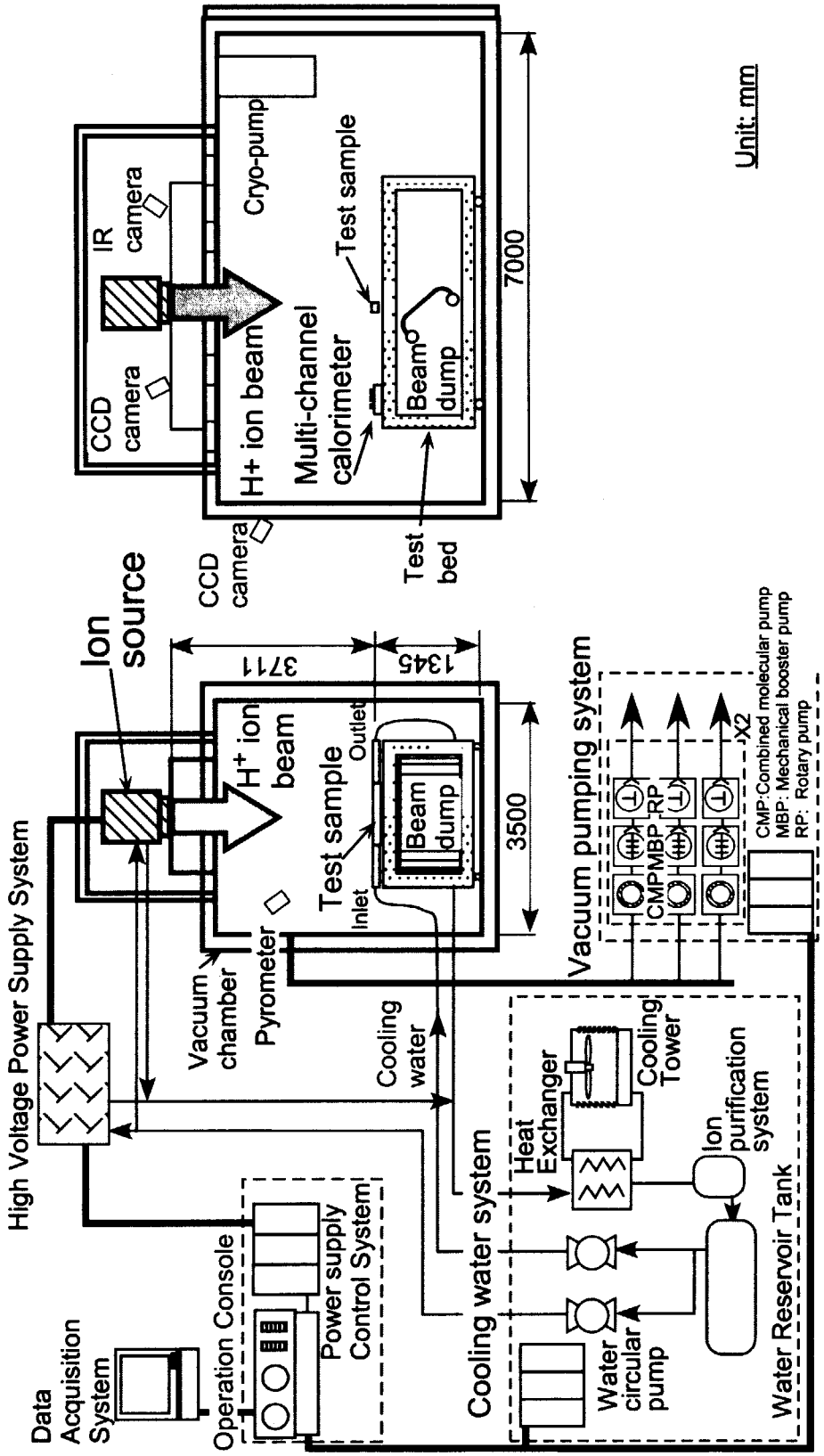

Figure 2-1 Schematics of PBEF of JAERI.

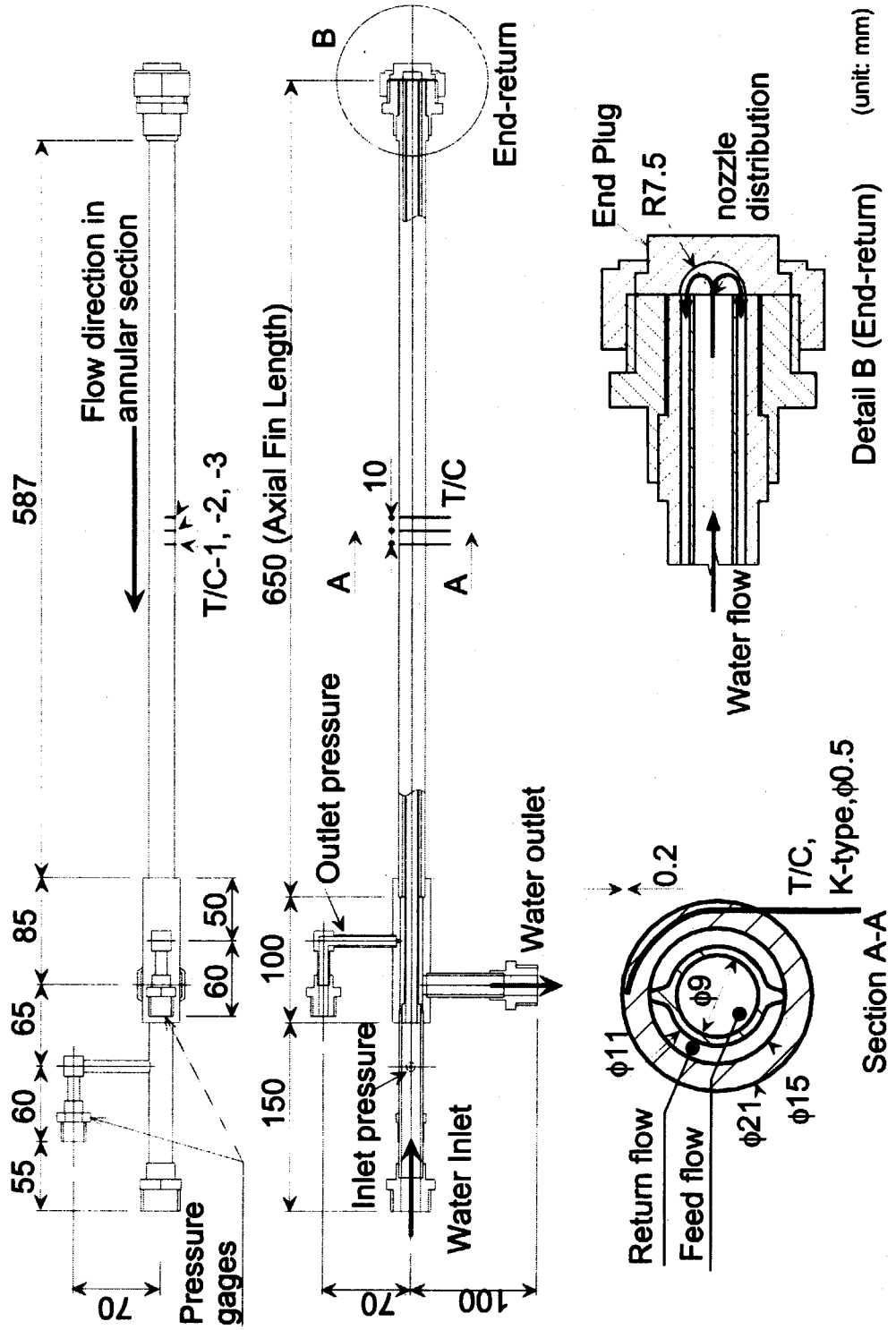

Figure 2-2 Annular tube mock-up for CHF and pressure drop experiments.

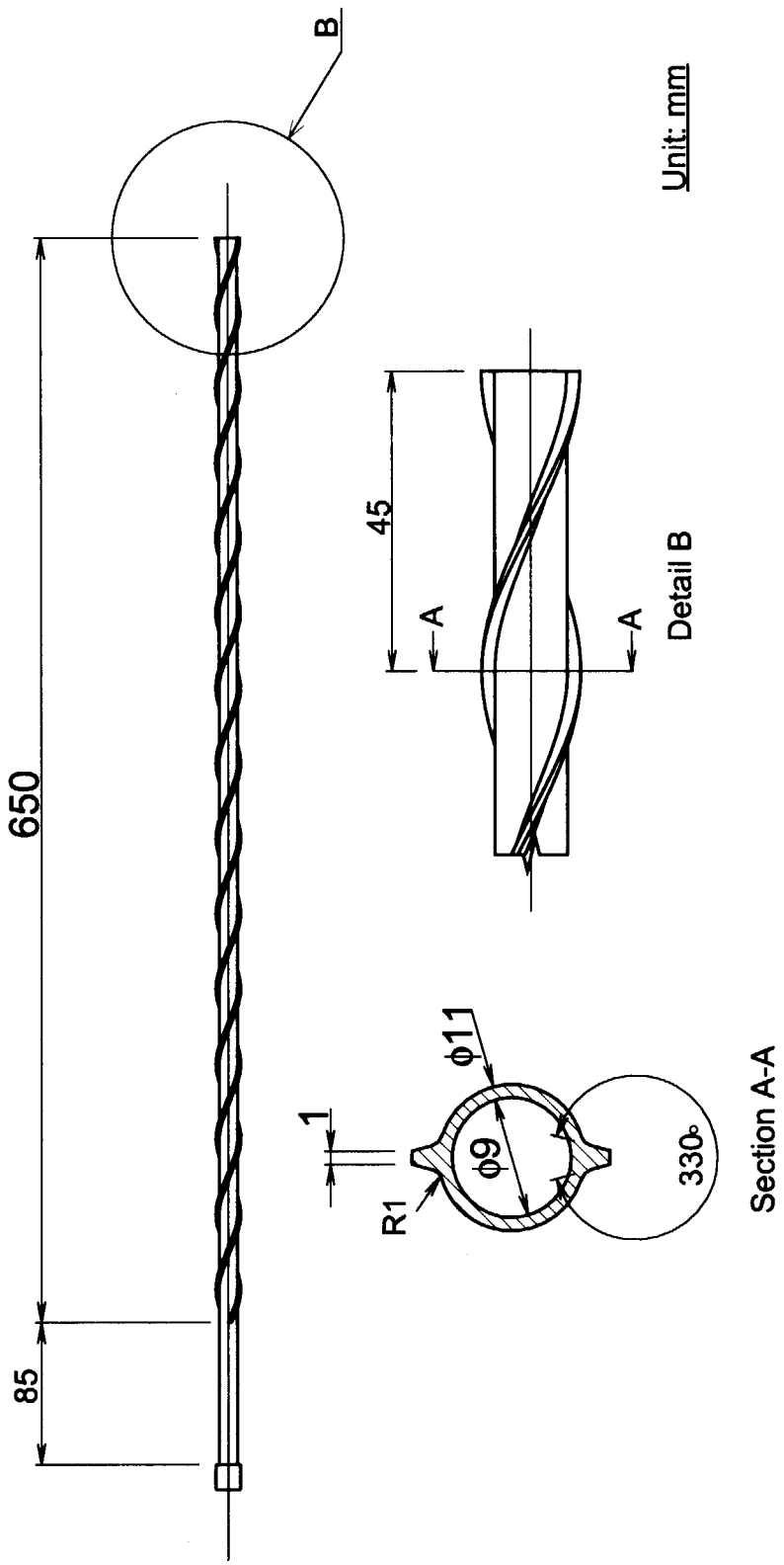

Figure 2-3 Details of inner tube with external swirl fins.

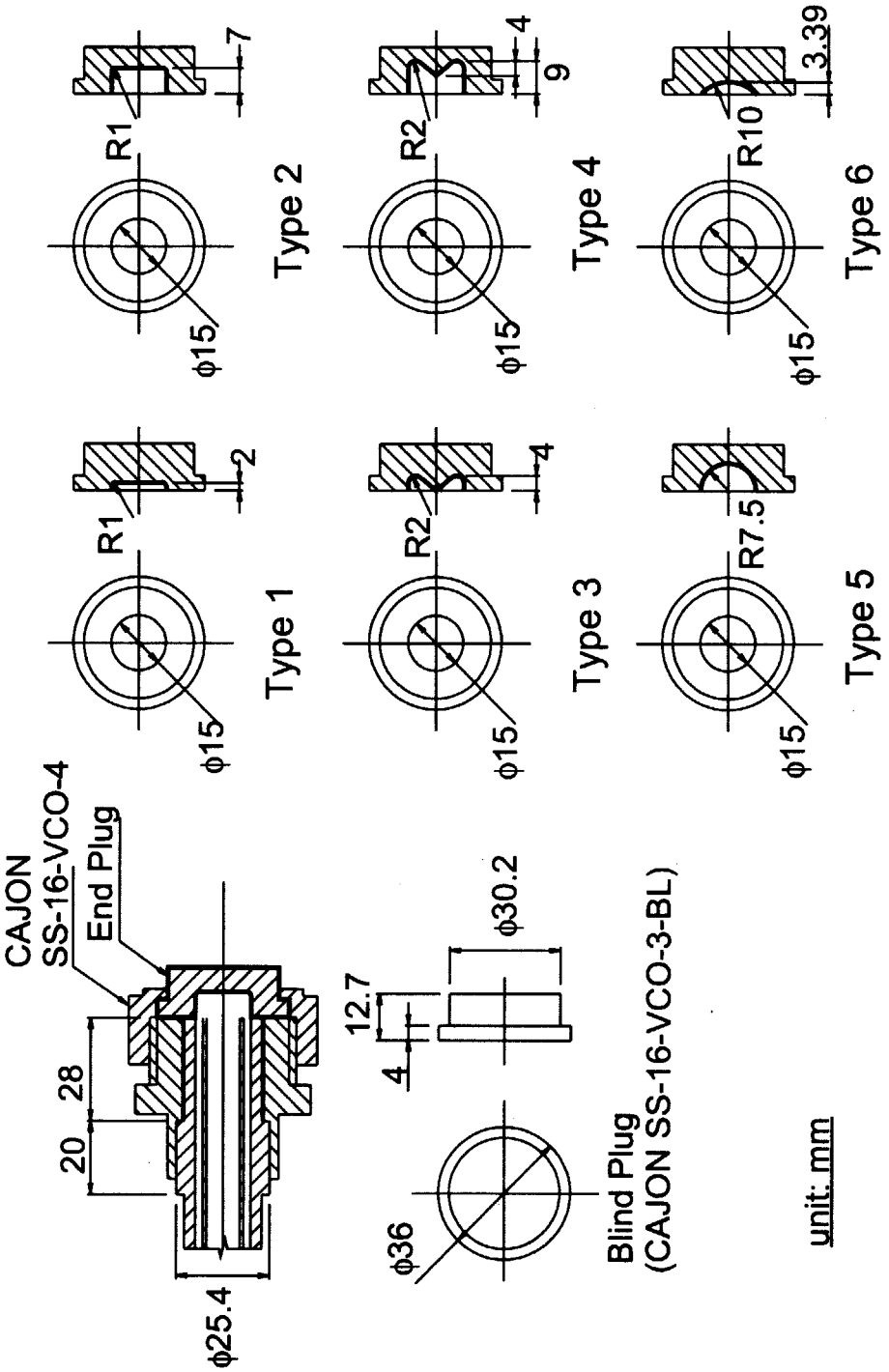

Figure 2-4 Detailed specifications of end-plug for end-return.

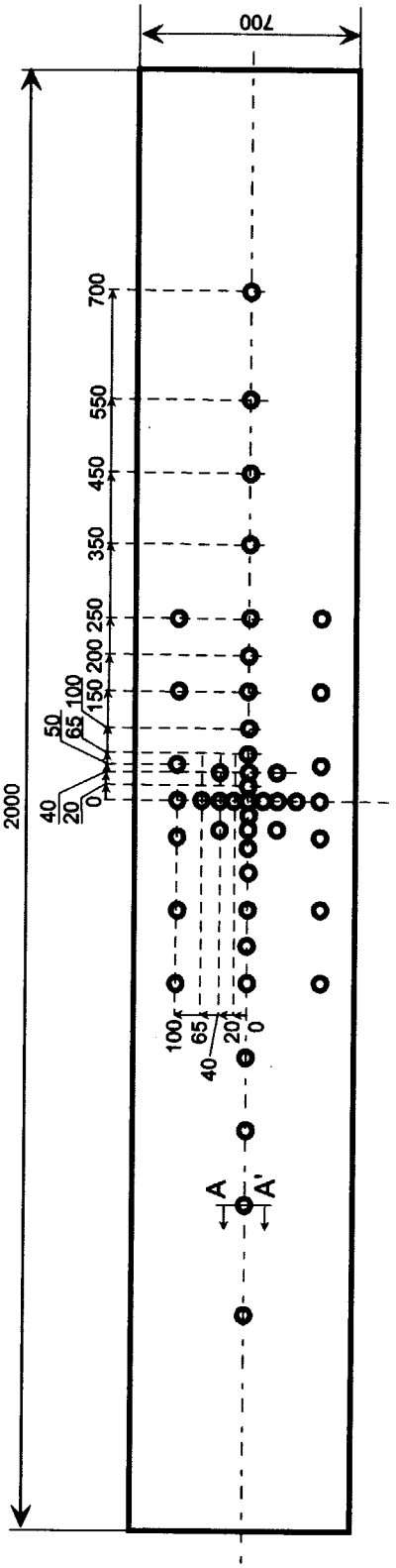

(a) Arrangement of calorimeter chips.

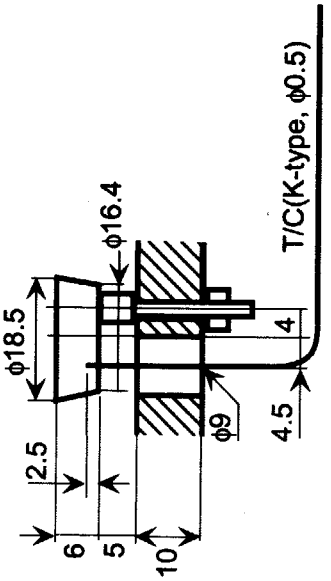

(b) Detail of calorimeter chip.

Cross-section A-A'

unit: mm

Figure 2-5 Details of multichannel calorimeter.

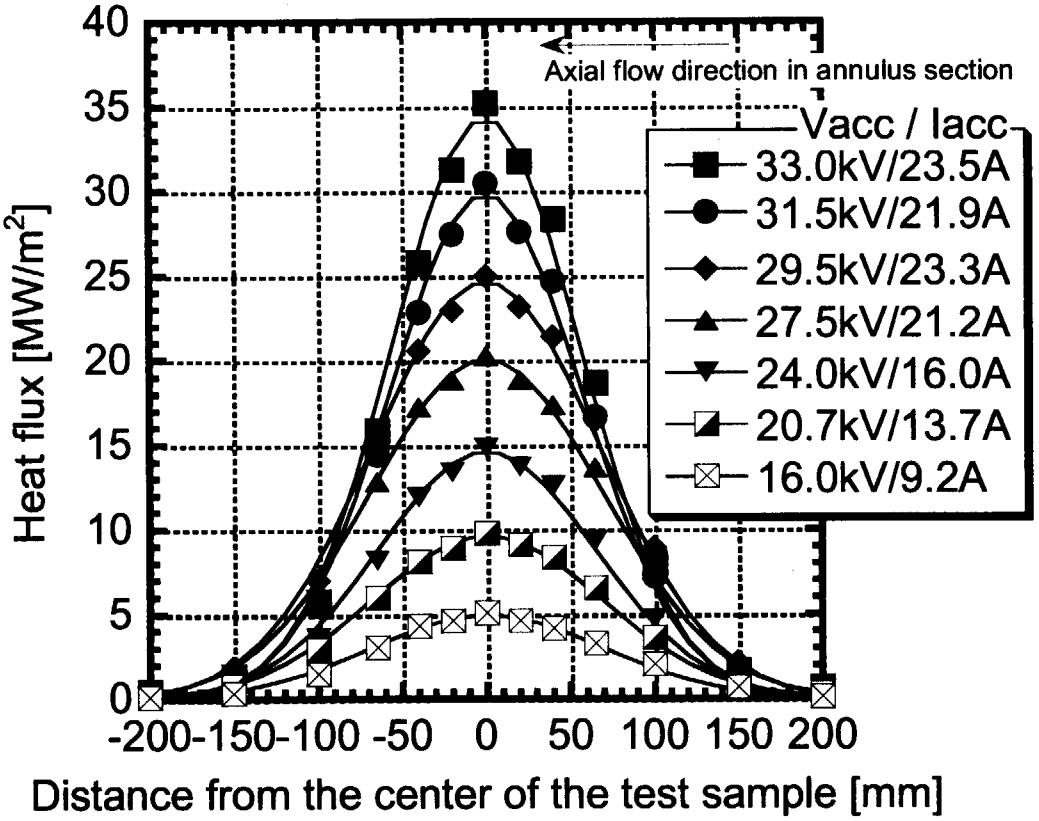

Figure 2-6 Typical heat flux profile at the test sample position.

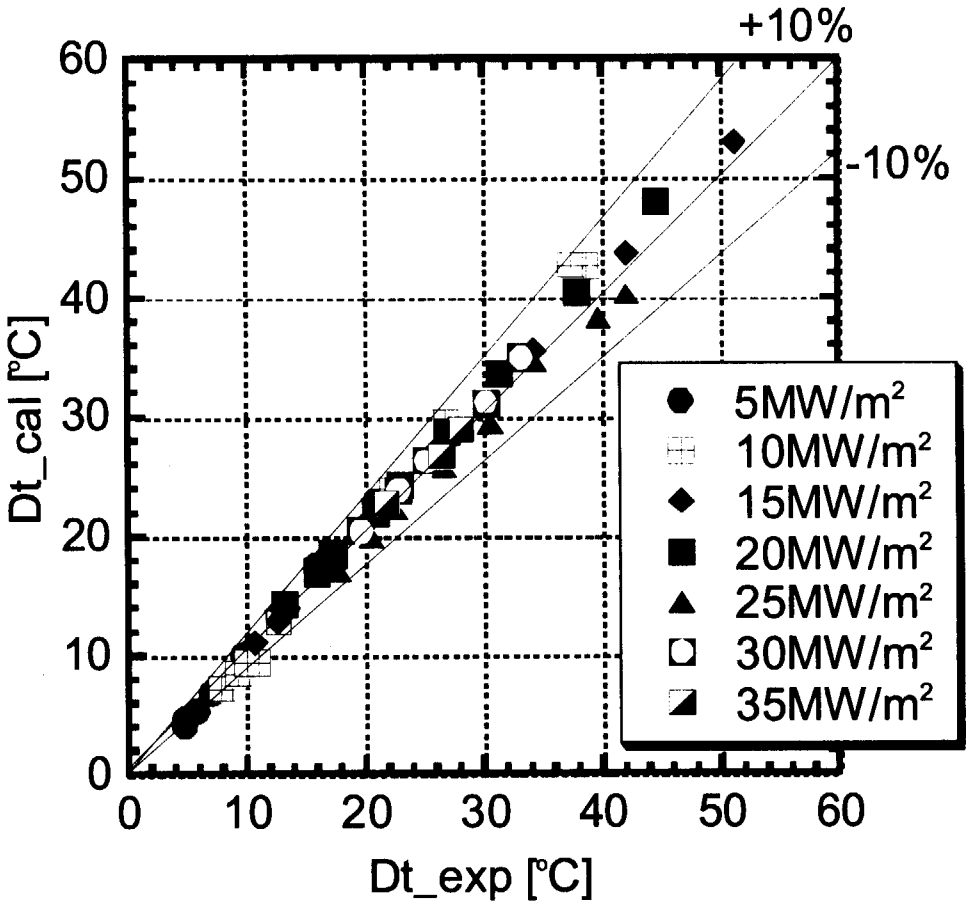

Figure 2-7 Typical heat flux profile at the test sample position.

3. Results and discussion

3.1. Pressure drop experiments

To confirm the capability of the pressure drop estimation in each flow section of the mock-up with the correlations mentioned in Sec. 2.4, the pressure drops in the inner smooth and outer annular tubes are measured separately. The measured pressure drops in both cases are compared with results estimated by the correlations. Figure 3-1 shows the results of the pressure drop experiments in the inner smooth tube section. Dashed, solid and dotted lines show the pressure drops estimated with the correlations (2-1)-(2-5) and correspond to the inlet, inner smooth, and outlet tube sections, respectively. The inlet and outlet sections have the expansion and contraction of the flow path as shown in Fig, 2-2. Solid circles represent the experimental results for the whole test section. The sum of calculated pressure drops is in good agreement with the experimental ones. This shows that the present method for estimation of the pressure drop is appropriate not only in the inner smooth tube section but also in the inlet and outlet sections of the test sample.

Figure 3-2 shows the pressure drops in the outer annular section with twisted fins. The same method as Fig 3-1 is used to estimate the pressure drops in the inlet and outlet tube sections. To estimate the pressure drop in the annular section, the equations (2-6)-(2-10) are applied. The sums of the calculated pressure drops are over-estimated compared with the experimental ones. These differences might be depended on the ability to predict the pressure drop, especially, the friction factor in the annular section. In order to estimate the pressure drop at the end-return, a new correlation must be made for this experiment. For this purpose, the friction factor is estimated based on the pressure drop data in the annular section, which is obtained by subtracting the inlet and outlet tube sections from the experimental results shown in Fig. 3-2. The friction factors estimated in the annular section are plotted in Fig. 3-3. Based on these data, a new correlation of the friction factor for the annulus with the twisted fin is derived using the following equation of which the equation form is the same as CEAís one, and it is expressed by,

$$\lambda = 0.0725 \mathrm{Re}_{H,sw}^{-0.1225} \qquad (3\text{-}1)$$

Applying this correlation, the experimental and calculated pressure drops in whole section of the annular swirl tube mock-up with the end-return are compared in Fig. 3-4. Finally the pressure drops at the end-return are estimated in Fig. 3-5 as functions of the volumetric flow rate and the average axial flow velocity in the annular section. In the low flow rate region (< 30 l/min), the pressure drop at the end-return provided by each end plug shows almost the same value. In higher flow rate region, however, the pressure drop provided by the Type-5 end-plug is the least value among all test data. The Type-5 end-plug has a semi-spherical shape with a radius of 7.5 mm, which is the same as the radius of the outside tube. The pressure drop in case of Type-5 end-plug is estimated about 0.09 MPa at the velocity of 10 m/sec, which accounts for about 17% of the total pressure drop of the test sample as shown in Fig. 3-4.

To compare the pressure drop of the annular section with that of the conventional swirl tube, Fig. 3-6 shows the pressure drop per unit length of each tube as a function of the average axial flow velocity. As a reference of the pressure drop of the conventional swirl tube, the results are compared with the correlation proposed by Manglik and Bergles for the conventional swirl tube [5],

$$f_{\text{fanning}} = \frac{0.791}{\text{Re}^{0.25}}\left(\frac{\pi}{\pi - 4\delta_t/d}\right)^{1.75}\left(\frac{\pi + 2 - 2\delta_t/d}{\pi - 4\delta_t/d}\right)^{1.25}\left(1 + \frac{2.752}{T_R^{1.29}}\right) \tag{3-2}$$

$$\frac{\Delta P}{\Delta x} = f_{\text{fanning}}\frac{2\rho U_{ax}^2}{d} \tag{3-3}$$

where, f_{fanning}, δ_t, d and $\Delta P/\Delta x$ are the fanning friction factor, thickness of twisted tape, inner diameter of empty tube and pressure drop per unit length, respectively. For the conventional swirl tube, the experimental and estimated pressure drops agree well. This indicates the validation of the pressure drop measurement of the conventional swirl tube. The pressure drops in the annular section in the whole axial flow velocity range are larger than those of the conventional swirl tube. Typically, the pressure drop in the annular section at 10 m/sec is about 1.9 times larger than that of the swirl tube. One of some reasons for this is the smaller hydraulic diameter of the annular swirl tube, D_H = 3.54 mm, than those of the conventional swirl tube, D_H = 8.97 mm.

From the engineering viewpoint, pumping power to supply the specified cooling water is one of the important parameters in the design of adequate cooling systems. Figure 3-7 shows the pumping power per unit length as a function of the axial flow

velocity. The pumping power is defined as the product of the pressure drop per unit length and the volumetric flow rate. The pumping powers to circulate the cooling water in the annular section and the conventional swirl tube under the same axial velocity condition are almost the same value although the pressure drop in the annular section with the twisted fin is a little larger than those of the conventional swirl tube. This reason is that the smaller volumetric flow rate in the annular swirl tube is required to obtain the specified axial flow velocity in comparison with those of the conventional swirl tube. The cross-section of the annular section is 46% of that of the present conventional swirl tube.

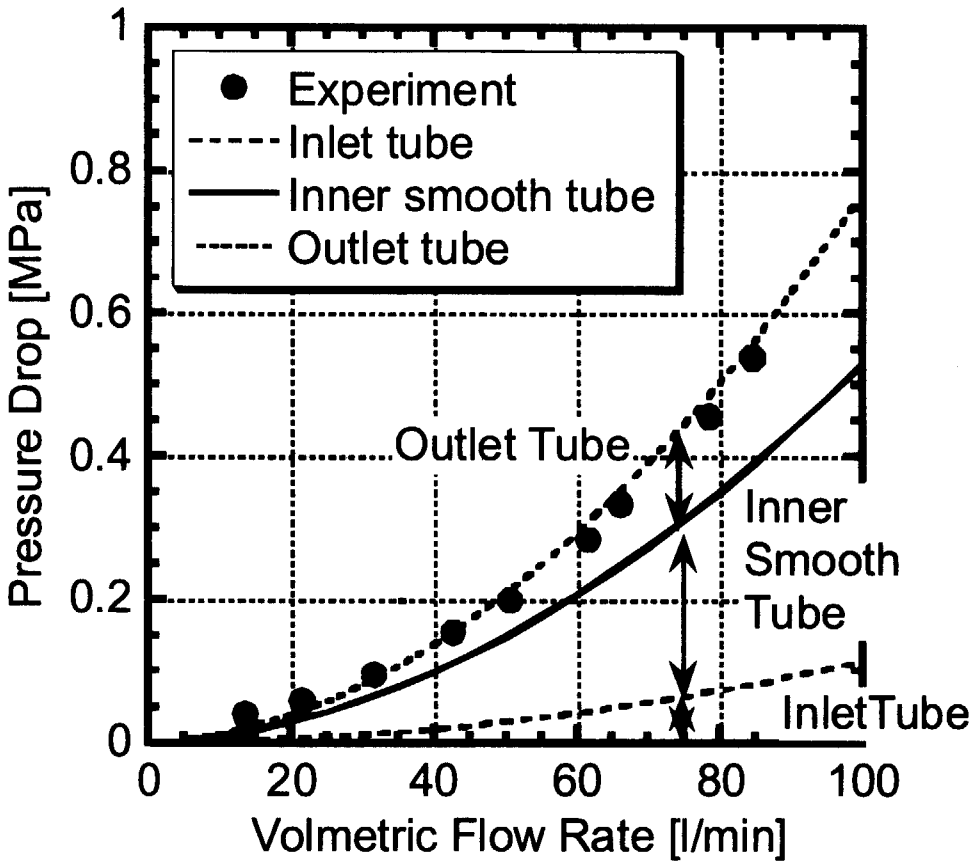

Figure 3-1 Pressure drop in the inner smooth tube section.

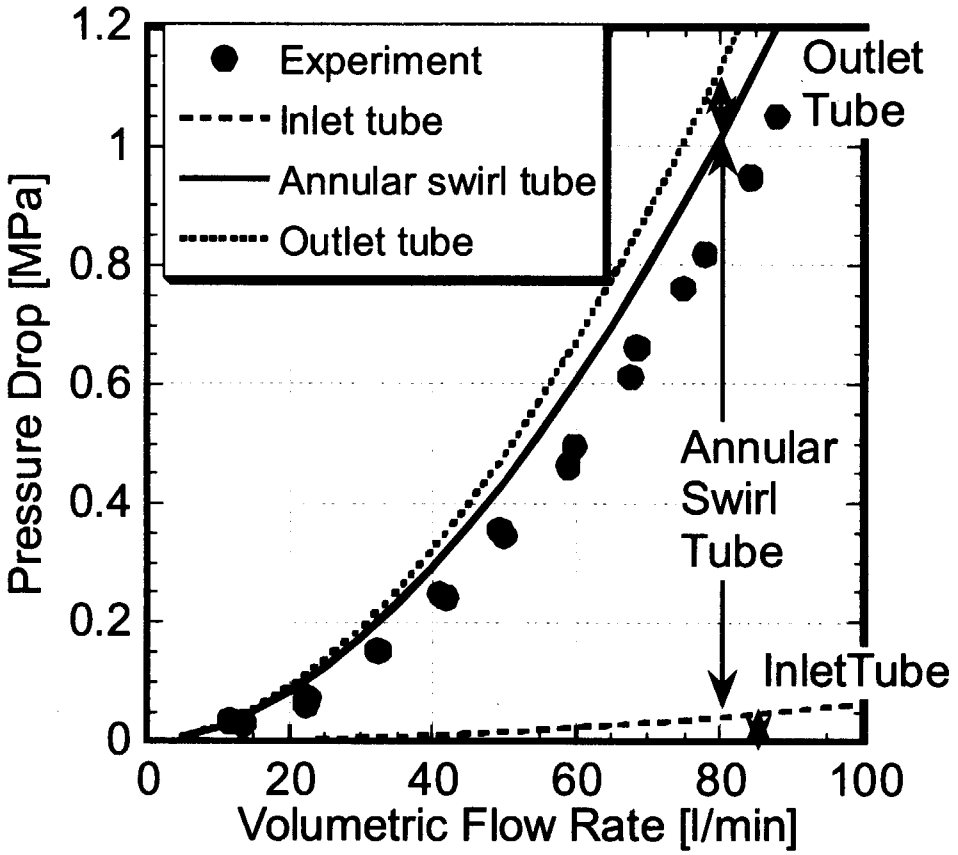

Figure 3-2: Pressure drop in the outer annular section with twisted fins.

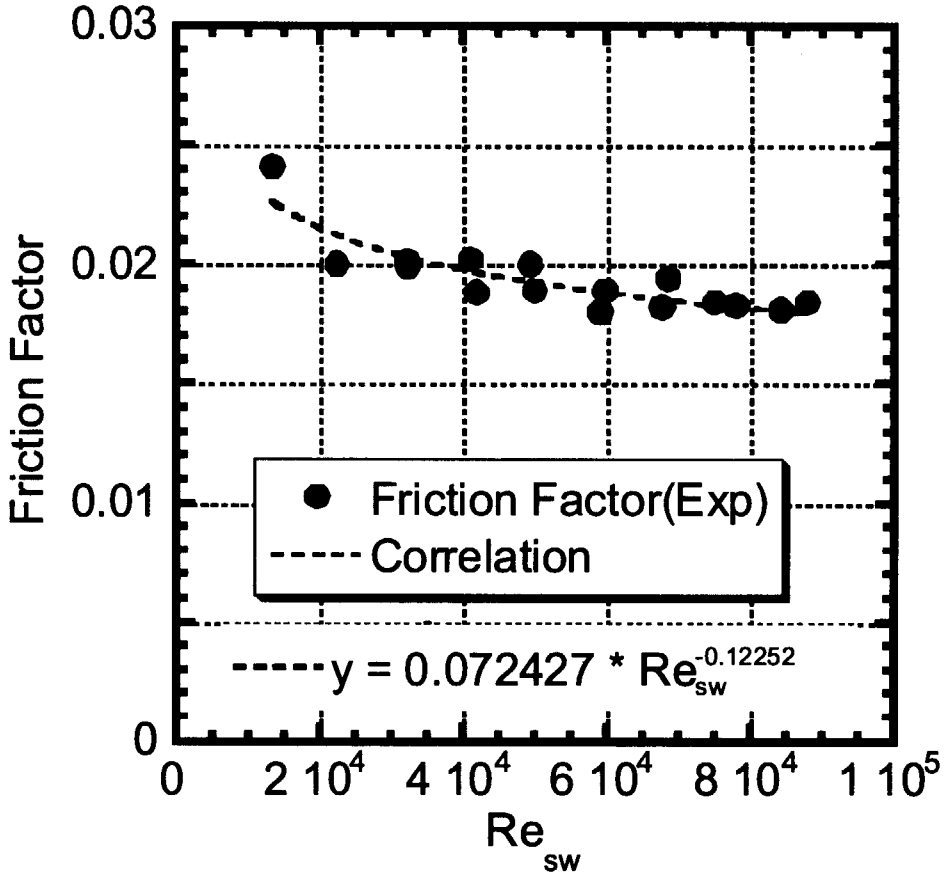

Figure 3-3 Friction factor in the annular tube section with twisted fins.

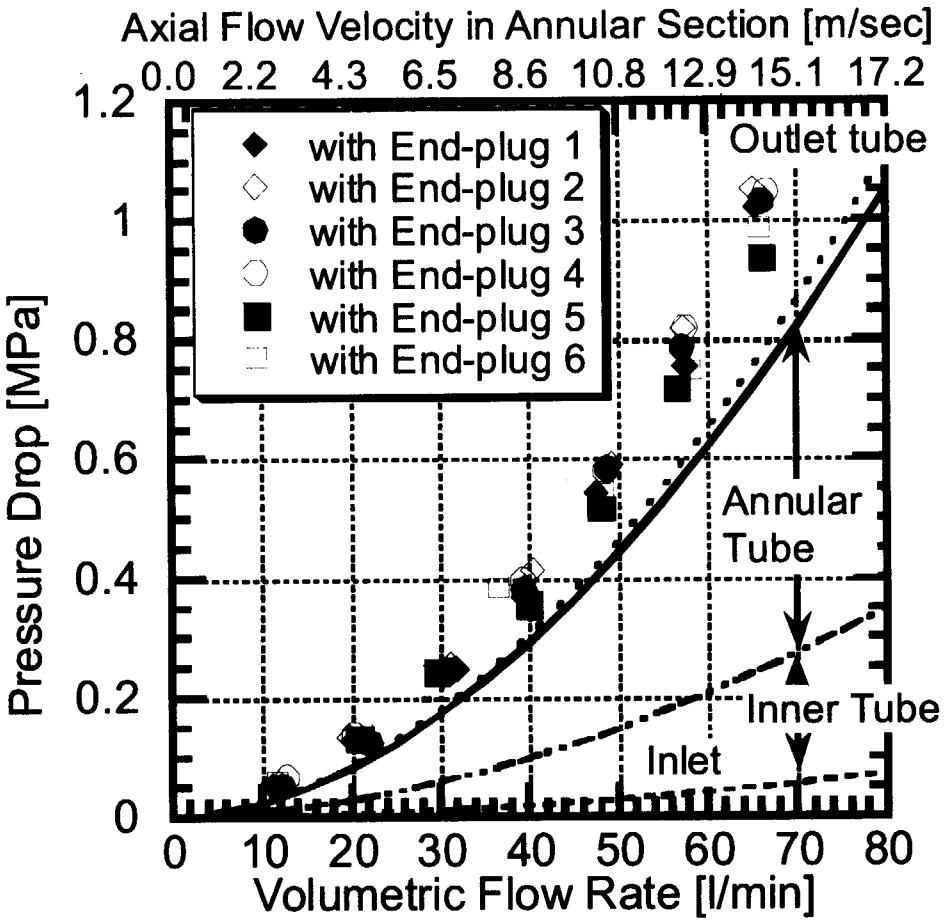

Figure 3-4 Pressure drop in whole section of mock-up including end-return.

Here, the volumetric flow rate can be expressed by using the axial flow velocity. For instance, 80 l/min corresponds to 17.2 m/s as can be seen in this figure.

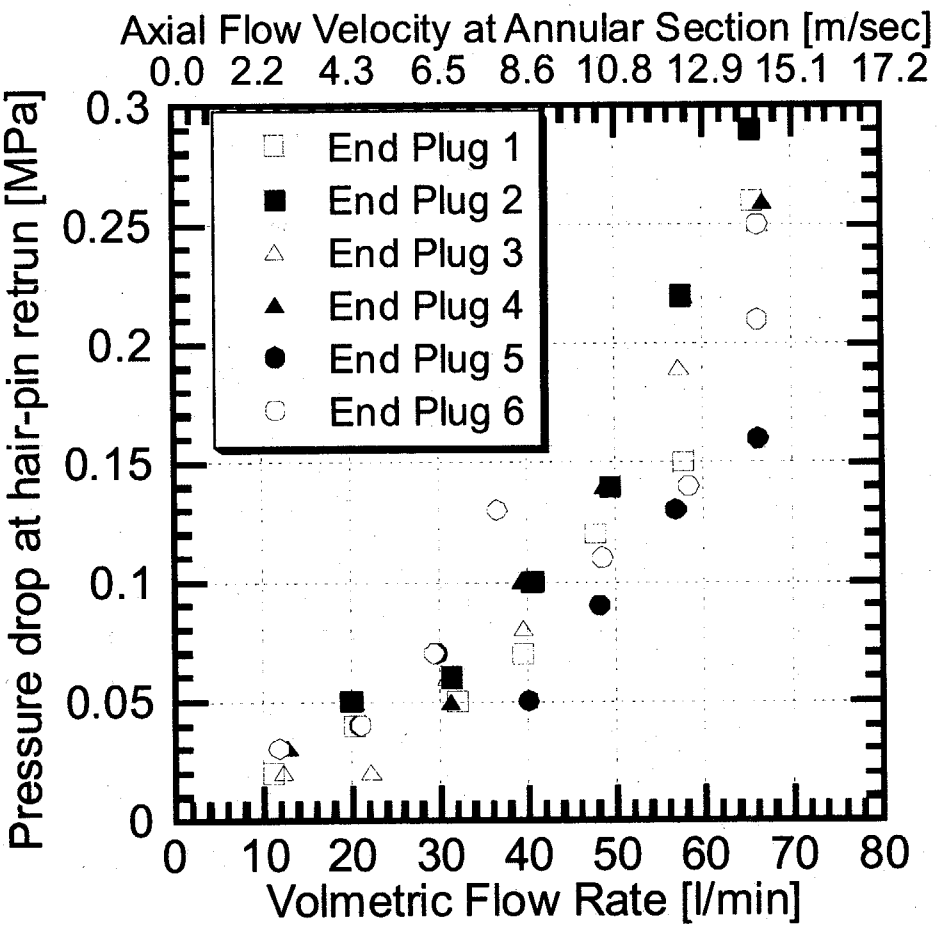

Figure 3-5: Pressure drop at the end-return section.

Here, the volumetric flow rate can be expressed by using the axial flow velocity. For instance, 80 l/min corresponds to 17.2 m/s as can be seen in this figure.

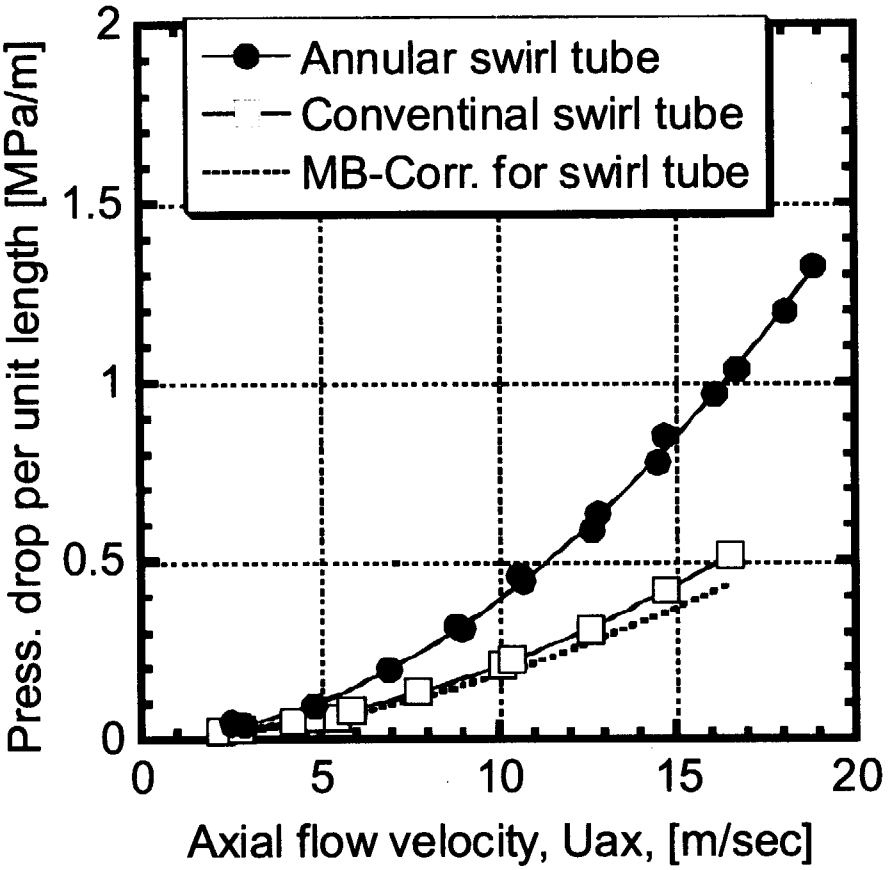

Figure 3-6: Pressure drop per unit length of the annular section with twisted fin and the conventional swirl tube as a function of axial flow velocity.

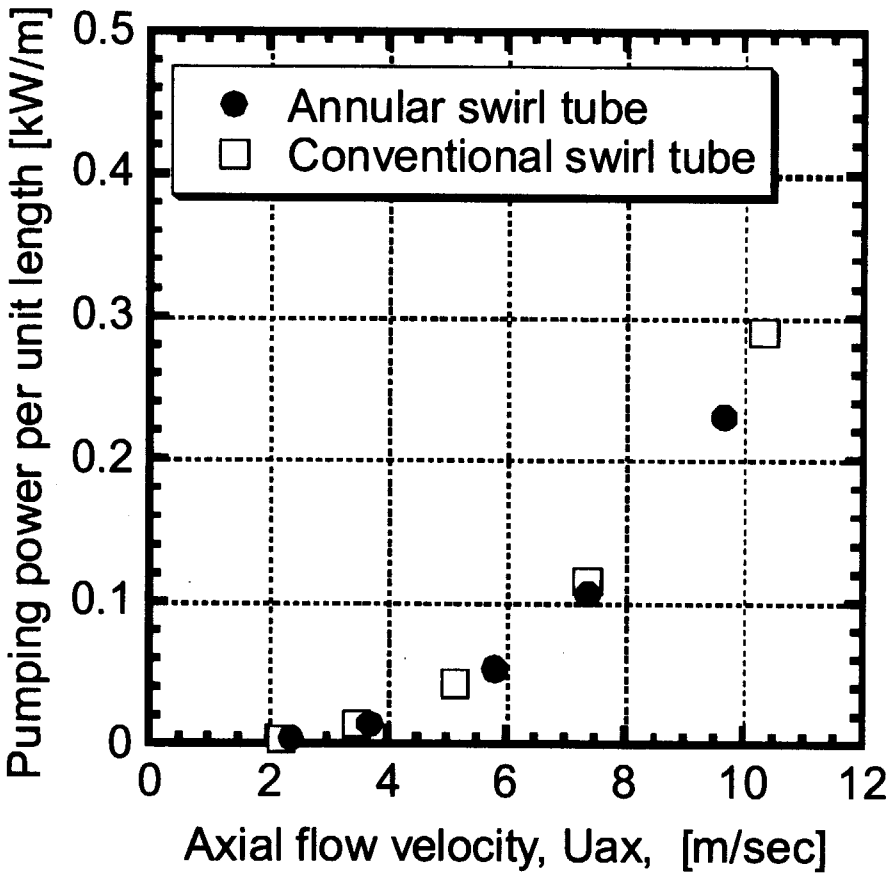

Figure 3-7: Pumping power to circulate the cooling water to the annular section with twisted fin and the conventional swirl tube as a function of axial flow velocity.

3.2. Critical heat flux experiments

Tables 3-1 and 3-2, and Tables 3-3 and 3-4 summarize the experimental conditions and heating test results on the annular swirl tube and the conventional swirl tube, respectively. These tables include incident heat flux (IHF), time to reach burnout ($T_{burnout}$), volumetric flow rate (V), axial flow velocity (Uax), inlet and local pressure, (P_{in} and P_{local}), inlet and local temperature of cooling water (T_{in} and T_{local}), measured and calculated temperature rises of cooling water (Dt_exp and Dt_wtr), local saturation temperature of cooling water at P_{local} (Tsat), local subcooling ($T_{sub} = T_{sat}-T_{local}$), and mean wall temperatures measured with thermocouples at the steady state during heating test (TC-1, TC-2, and TC-3).

In general, CHF is defined at the inner wall of the cooling tube. However, the incident critical heat flux (ICHF), which is defined at the outer surface of the test sample, is considered here because of the one-sided-heating conditions. Figure 3-8 shows the typical temperature responses measured with thermocouple inserted into the top of the test sample for different axial positions. After reaching steady-state temperature within 5 sec from the start of the heating, wall temperature rapidly increased within several seconds due to an occurrence of burnout. Because the test sample is exposed to relatively wide ion beams, the CHF event is caught by the thermocouples, TC-1, TC-2 and TC-3 in turn. They are located at 10 mm downstream from the center of the test sample, the center, and 10 mm upstream from the center, respectively. This may result from a rapid spread of dryout on the inner wall of the tube from downstream to upstream of the coolant.

Figure 3-9 shows ICHF for the annular swirl tube as a function of the axial flow velocity at the annular section. At heat fluxes of 5 and 10 MW/m^2, the burnout did not occur in a low axial velocity region as 2.5 m/sec. ICHFs of the annular swirl tube are compared with those of the conventional swirl tube that has the same tube geometry as the outer tube of the annular swirl tube and the same twist ratio of the swirl tape. For both cooling tubes, ICHF increased with increasing the axial flow velocity. From these results, we can conclude that there is no degradation of ICHF for the annular swirl tube in comparison with the swirl tube at the experimental axial flow velocity range. This might result from the centrifugal or acceleration force due to the twisted motion of the cooling water by the twisted fin that has the same effect as the swirl tape inside the

swirl tube on enhancement of CHF, although small gap exists between the inner wall of the outer tube and the twisted fin in the annular swirl tube.

Comparing ICHF as a function of the pumping power that is needed to supply the required cooling water is important from viewpoint of global performance of cooling tubes. Using the pumping power data showed in Fig, 3-7, Fig. 3-10 shows repotted ICHF data by a pumping power that is required to supply the specified cooling water for a test section with 1 m in length. For the annular swirl tube, the pumping power is only estimated in the outer annular section with the twisted fins. The ICHF performance increases with the pumping power in both cooling tubes. From the viewpoint of the pumping power, it is found that they have almost the same ICHF performance, although the pressure drop in the annular section with the twisted fin is larger than those of the conventional swirl tube. From this result, it is evident that the volumetric flow rate required to obtain the specified ICHF for the annular swirl tube is smaller than those for the conventional swirl tube.

3.3. Thermal analyses with FEM and comparison of CHF correlations

In the previous section, we can confirm experimentally the heat removal limitation, that is, ICHF for the annular swirl tube is almost similar to those of the conventional swirl tube. In this section, the heat transfer performance for the annular swirl tube is discussed through examination of the applicability of heat transfer correlations of JAERI [6] first. For this purpose, the wall temperatures measured with the thermocouples are compared with the numerical results using ABAQUS code [7] with the finite element method (FEM). In addition, applicability of existing correlations for CHF to the results of the annular swirl tube is examined, which is important factor from the viewpoint of design study of the high heat flux components using the annular swirl tube.

The heat transfer correlations used in the present analyses are follows [6],

For forced convection regime for swirl tube;

$$\mathrm{Nu}_s = 0.023\,\mathrm{Re}_H^{0.8}\,\mathrm{Pr}^{0.4}\times\left(2.18/T_R^{0.09}\right)\times\left(\mu/\mu_{wall}\right)^{0.14}, \qquad (3\text{-}4)$$

For sub-cooled nucleate boiling regime;

$$T_{wall} - T_{sat} = 25.72\times q^{1/3}/\exp(p/8.6), \qquad (3\text{-}5)$$

where, Nu_s is Nusselt number ($= h D_H / \kappa$) for the swirl tube, which is the Dittus-Boelter correlation multiplied by Gambilís swirl factor [8] and wall viscosity factor. In addition, h, k, Pr, and μ_{wall} are the heat transfer coefficient, thermal conductivity and Prandtl number of water at the bulk water temperature, and the viscosity of water at the wall temperature. Hydraulic diameters D_H are 3.54 mm for the annular swirl tube and 15 mm for the conventional swirl tube. Bulk temperature rises at the center of the test samples as summarized in Tables 3-1 to 3-4 are estimated from the input power profiles and the flow rate and they are taken into estimating the heat transfer coefficients. The typical heat transfer coefficients temperatures are shown as a function of the inner wall temperature in Fig. 3-11.

Using these heat transfer coefficients, the heat conduction analyses in the outer tube are performed in a two-dimensional FEM model. Boundary conditions are shown in Fig. 3-12. For the annular swirl tube, only the outer tube is taken into analyses because the inner tube contributes as only a turbulence promoter, and no heat sink for the outer tube. Tables 3-5 and 3-6 summarize the results of numerical results for the annular swirl and the conventional swirl tubes. These include IHF, Uax, wall temperature at the thermocouple position (TC) and the inner wall (T_{wall}), wall heat flux (WHF), heat transfer coefficient, and peaking factor of WHF to IHF.

Figure3-13 shows the comparison of numerical results with experimental ones for the annular swirl tube. In the present experiments, until the burnout phenomenon occurred at the given heat flux condition, the axial flow velocity decreased step by step from a high velocity to a low velocity region, that is, from right to left in this figure. The axial velocities represent 2.4, 3.7, 5.8 7.4 and 9.7 m/s at the heat flux conditions of 20, 25, 30 and 35 MW/m^2 at the burnout. The analytical results are in good agreement with the experimental ones in the whole experimental conditions, which indicate that the correlation for heat transfer coefficient is applicable enough to predict the thermal performance of the annular swirl tube.

At low heat flux condition, i.e., at 5 MW/m^2 for the annular swirl tube, the wall temperature increased monotonously with the decreasing of the axial flow velocity. On such thermal-hydraulic conditions, the forced convective heat transfer is dominant and the heat transfer coefficient is proportional to the axial flow velocity. In a higher heat flux condition of more than 25 MW/m^2, the wall temperature depends slightly on

the axial flow velocity. In these conditions, the nucleate boiling is dominant in the heat transfer, in which heat removal mechanism has little dependence on the flow velocity of the coolant. In the intermediate heat flux conditions from 10 to 20 MW/m^2, the wall temperatures approaches a constant value with decreasing of the flow velocity. In these thermal-hydraulic conditions, the dominant heat transfer mechanism varies from the forced convection at the higher flow velocity region to the nucleate boiling at the lower flow velocity region.

Figure 3-14 shows the comparison of the numerical results with experimental ones for the conventional swirl tube. The transitions of the heat transfer regimes are also observed like those of the annular swirl tube shown in Fig. 3-13. By comparison of the wall temperatures of the annular swirl tube with those of the conventional swirl tube under the given thermal-hydraulic conditions, they are almost coincident. Therefore, we can conclude that there is no degradation of the heat removal performance of the annular swirl tube compared with those of the conventional swirl tube.

Using numerical results, wall critical heat flux (WCHF) at the burnout can be determined. Maximum wall heat flux appeared at the top of the inner wall and the peaking factor of WCHF/ICHF increases from 1.28 to 1.36 according to the incident heat flux. These values are necessary to compare the present experiments with the correlated values. Because the CHF correlations can usually predict WCHF, although it cannot predict ICHF. In the present study, WCHFs are compared with the following two CHF correlations; one is Tong-75 correlation, which is originally developed for the light-water fission reactor [9]. This correlation has been extensively used to estimate WCHF and also applied in the design analysis of ITER divertor [2]. The other is one proposed by Boscary et al. to predicting WCHF for smooth and swirl tubes based on dimension analyses of CHF phenomena under one-sided heating conditions [10]. These tow correlations are formulated in term of Boiling number as follows,

In TONG-75 correlation;

$$\mathrm{Bo}_c = 0.23 f \left[1 + 0.00216 \left(\frac{P}{P_c} \right)^{1.8} \mathrm{Re}_H^{0.5} J_a \right], \tag{3-6}$$

In Boscary, et alís correlation;

$$\mathrm{Bo}_c = \frac{1}{25} \exp\left(X_{sub}^2\right) \left[\mathrm{Ec}_{sw}^{-1/7} \mathrm{Re}_{H,sw}^{-1/4} \mathrm{Rd}^{-1/4} \left(-X_{sub}\right)^{1/10} \right]. \tag{3-7}$$

Using above correlation, WCHF are estimated as follow,

$$\mathrm{WCHF} = \rho_L U_{ax} \Delta h_v \, \mathrm{Bo}_c . \tag{3-8}$$

where,

$$f = 8\,\mathrm{Re}_H^{-0.6} (D_H / D_o)^{0.32}, \tag{3-9}$$

$$\mathrm{Ja} = \frac{\rho_L}{\rho_g} \frac{C_p (T_{sat} - T_{local})}{\Delta h_v} , \tag{3-10}$$

$$X_{sub} = -\frac{C_p (T_{sat} - T_{local})}{\Delta h_v}, \tag{3-11}$$

$$\mathrm{Ec}_{sw} = \frac{Uax^2}{C_p (T_{sat} - T_{local})}, \tag{3-12}$$

$$\mathrm{Rd} = \frac{\rho_L}{\rho_g}, \tag{3-13}$$

Here, f is the friction factor, P is the local pressure of coolant, P_c is the critical pressure, 22.1 MPa, Ja is the Jakob number, X_{sub} is the mass enthalpic quality, $\mathrm{Ec_{sw}}$ is the Eckert number based on swirl velocity, Rd is the density ratio of liquid at $\mathrm{T_{local}}$, ρ_L and ρ_g are the water and vapor densities at $\mathrm{T_{sat}}$, Re_H is Reynolds number based on hydraulic diameter of tube and axial flow velocity, $\mathrm{Re}_{H,sw}$ is Reynolds number based on hydraulic diameter and swirl flow velocity, Δh_v is latent heat of vaporization of water, $\mathrm{D_o}$ is reference diameter (=12.7 10^{-3}), and C_p is specific heat of water at T_{local}.

Figures 3-15 and 3-16 and Figs. 3-17 and 3-18 show the ratio of the experimental WCHFs to estimated values by the correlations by Tong and Boscary et al. as functions of axial flow velocity and local subcooling, $\mathrm{T_{sub}}$ (= $\mathrm{T_{sat}}$-$\mathrm{T_{local}}$). According to these correlations, WCHF is dependent on the flow velocity and local subcooling. From these results, both correlations could predict well the experimental results within an error of ± 20% error margin in the present experimental range. These results show the applicability of these correlations to predict WCHF for the conventional swirl tube as well as the annular swirl tube.

Table 3-1 Experimental conditions and results of CHF test on the annular swirl tube (1).

Data name	IHF	$T_{burnout}$	V	Uax	Pin	Plocal	Tin	Tlocal	Dt_exp	Dt_wtr	Tsat	Tsub	TC-1	TC-2	TC-3
	[MW/m^2]	[sec]	[l/min]	[m/sec]	[MPa]	[MPa]	[°C]	[°C]	[°C]	[°C]	[°C]	[°C]	[°C]	[°C]	[°C]
0728_001	10.0		120.5	11.9	1.01	1.00	29.4	32.1	5.4	4.3	179.7	147.7	242.9	243.1	248.9
0728_002	10.0		103.3	10.2	1.04	1.05	29.4	32.4	6.1	5.0	182.2	149.8	256.6	257.6	265.8
0728_003	10.0		80.3	7.9	0.93	0.98	29.4	32.9	7.1	6.5	178.9	145.9	274.6	272.0	275.1
0728_004	10.0		61.5	6.1	0.97	1.03	29.4	33.8	8.8	8.5	181.3	147.5	285.9	280.2	281.4
0728_005	10.0		40.2	4.0	1.06	1.13	29.4	35.7	12.7	13.0	185.4	149.7	296.9	291.3	290.3
0728_006	10.0		21.6	2.1	1.02	1.11	29.4	40.4	22.0	24.1	184.3	144.0	300.8	296.4	293.7
0728_007	10.0		15.3	1.5	0.95	1.05	29.4	44.6	30.5	34.0	181.9	137.3	300.6	296.2	293.5
0728_008	10.0		11.5	1.1	1.06	1.15	29.4	49.6	40.4	45.2	186.1	136.5	301.4	294.7	293.6
0728_010	10.0		11.5	1.1	1.11	1.21	29.4	50.8	42.9	45.4	188.3	137.5	304.3	296.9	296.2
0728_009	10.0		11.2	1.1	1.11	1.21	29.4	50.9	43.1	46.4	188.2	137.3	304.4	296.9	296.1
0728_011	15.0		120.8	11.9	1.06	1.05	29.4	32.9	7.2	6.1	182.0	149.1	325.3	322.1	326.4
0728_012	15.0		101.5	10.0	1.01	1.03	29.4	33.3	7.8	7.2	181.4	148.1	331.7	327.1	328.9
0728_013	15.0		81.3	8.0	1.07	1.11	29.4	34.3	9.8	9.0	184.6	150.3	343.2	335.4	335.4
0728_014	15.0		60.3	5.9	1.02	1.09	29.4	35.7	12.6	12.1	183.8	148.1	344.7	338.3	336.8
0728_015	15.0		40.0	3.9	0.89	0.98	29.4	38.4	18.1	18.3	178.8	140.4	343.2	337.3	335.4
0728_020	15.0		27.2	2.7	1.04	1.13	29.4	44.9	31.2	26.8	184.1	140.3	346.5	335.8	336.0
0728_016	15.0		26.2	2.6	1.01	1.10	29.4	45.0	31.4	27.9	184.9	140.1	345.2	334.0	333.5
0728_019	15.0		25.0	2.5	1.04	1.13	29.4	45.0	31.3	29.3	185.2	140.0	345.2	335.3	335.4
0728_018	15.0	4.5	22.4	2.2	1.03	1.12	29.4	45.0	31.2	32.6	185.3	139.1	600.0	600.0	600.0
0808_017	20.0		120.7	11.9	1.00	1.02	29.4	33.7	8.7	7.8	180.8	147.1	400.0	389.5	390.3
0804_001	20.0		120.4	11.9	1.03	1.04	29.4	33.3	7.8	7.8	181.7	148.5	387.8	382.2	385.6
0808_016	20.0		100.9	9.9	1.02	1.07	29.4	34.3	9.8	9.3	182.7	148.5	405.6	394.7	395.4
0808_015	20.0		80.1	7.9	1.00	1.08	29.4	35.5	12.2	11.7	183.1	147.6	408.8	398.1	398.2
0808_014	20.0		59.2	5.8	1.00	1.09	29.4	37.4	16.1	15.8	183.8	146.4	409.9	399.0	399.3
0804_002	20.0		40.2	4.0	0.96	1.06	29.4	40.8	22.8	23.3	182.5	141.7	398.5	384.7	384.3
0804_004	20.0	8.3	35.4	3.5	0.96	1.07	29.4	42.3	26.0	26.4	182.7	140.4	600.0	600.0	600.0
0804_005	20.0	8.6	35.4	3.5	0.96	1.07	29.4	42.3	25.9	26.4	182.7	140.3	600.0	600.0	600.0
0804_003	20.0	5.0	30.0	3.0	0.96	1.06	29.4	42.8	26.8	31.2	182.4	139.7	600.0	600.0	600.0

Table 3-2 Experimental conditions and results of CHF test on the annular swirl tube (2).

Data name	IHF	$T_{burnout}$	V	Uax	Pin	Plocal	Tin	Tlocal	Dt_exp	Dt_wtr	Tsat	Tsub	TC-1	TC-2	TC-3
	[MW/m^2]	[sec]	[l/min]	[m/sec]	[MPa]	[MPa]	[°C]	[°C]	[°C]	[°C]	[°C]	[°C]	[°C]	[°C]	[°C]
0808_011	25.0		104.9	10.3	1.02	1.06	29.4	35.4	12.1	10.6	182.6	147.2	465.8	452.7	452.7
0808_012	25.0		80.1	7.9	1.00	1.07	29.4	37.3	15.9	13.9	183.1	145.7	468.6	452.0	450.5
0807_004	25.0		60.1	5.9	0.94	1.03	29.5	40.0	21.1	18.5	181.3	141.4	469.3	443.4	441.3
0807_003	25.0		59.9	5.9	0.94	1.03	29.4	40.0	21.3	18.6	181.2	141.2	470.5	443.3	441.0
0808_013	25.0		59.4	5.8	1.00	1.10	29.4	39.6	20.6	18.8	183.9	144.2	477.3	447.9	446.0
0807_005	25.0		56.0	5.5	0.98	1.08	29.4	40.6	22.5	19.9	183.2	142.6	485.2	458.0	493.0
0807_007	25.0	4.3	52.1	5.1	0.86	1.00	29.4	40.7	22.6	21.4	179.8	139.2	600.0	600.0	600.0
0807_006	25.0	3.6	50.1	4.9	0.84	0.94	29.4	40.5	22.2	22.2	177.2	136.7	600.0	600.0	600.0
0808_001	30.0		120.5	11.9	1.00	1.02	29.4	35.4	12.0	11.0	180.9	145.5	490.5	477.5	478.4
0807_010	30.0		120.1	11.8	0.95	0.96	29.4	35.7	12.7	11.1	178.2	142.5	502.7	492.4	490.2
0807_011	30.0		80.7	8.0	0.94	1.01	29.4	38.4	18.0	16.5	180.3	142.0	517.5	503.3	543.2
0807_012	30.0		80.7	8.0	0.94	1.01	29.4	38.4	18.1	16.5	180.5	142.1	518.8	505.1	547.2
0808_004	30.0		79.0	7.8	1.06	1.13	29.4	38.2	17.8	16.8	185.4	147.1	519.6	495.9	493.4
0808_003	30.0		79.0	7.8	1.06	1.13	29.4	38.4	18.1	16.8	185.4	147.0		497.6	496.9
0808_002	30.0		78.9	7.8	1.06	1.13	29.4	37.9	17.1	16.9	185.4	147.5		480.5	477.8
0807_013	30.0	4.6	74.9	7.4	1.02	1.09	29.4	38.6	18.6	17.8	183.7	145.1	600.0	600.0	600.0
0808_005	30.0	4.8	73.9	7.3	1.05	1.13	29.4	39.0	19.3	18.0	185.4	146.4	600.0	600.0	600.0
0808_006	30.0	5.3	69.8	6.9	1.04	1.13	29.4	39.2	19.6	19.0	185.2	146.0	600.0	600.0	600.0
0808_007	35.0		120.6	11.9	1.05	1.07	29.4	36.2	13.7	12.3	182.9	146.7	560.1	545.0	539.1
0808_009	35.0		109.8	10.8	1.05	1.09	29.4	36.7	14.6	13.5	183.6	146.9	560.2	545.6	562.5
0808_010	35.0	5.7	104.9	10.3	1.03	1.07	29.4	37.3	15.9	14.2	182.7	145.3	600.0	600.0	600.0
0808_008	35.0	4.1	98.9	9.7	1.00	1.06	29.4	37.3	15.9	15.0	182.4	145.1	600.0	600.0	600.0

Table 3-3 Experimental conditions and results of CHF test on the conventional swirl tube (1).

Data name	IHF	$T_{burnout}$	V	Uax	Pin	Plocal	Tin	Tlocal	Dt_exp	Dt_wtr	Tsat	Tsub	TC-1	TC-2	TC-3
	[MW/m^2]	[sec]	[l/min]	[m/sec]	[MPa]	[MPa]	[°C]	[°C]	[°C]	[°C]	[°C]	[°C]	[°C]	[°C]	[°C]
0728_001	10.0		120.5	11.9	1.01	1.00	29.4	32.1	5.4	4.3	179.7	147.7	242.9	243.1	248.9
0728_002	10.0		103.3	10.2	1.04	1.05	29.4	32.4	6.1	5.0	182.2	149.8	256.6	257.6	265.8
0728_003	10.0		80.3	7.9	0.93	0.98	29.4	32.9	7.1	6.5	178.9	145.9	274.6	272.0	275.1
0728_004	10.0		61.5	6.1	0.97	1.03	29.4	33.8	8.8	8.5	181.3	147.5	285.9	280.2	281.4
0728_005	10.0		40.2	4.0	1.06	1.13	29.4	35.7	12.7	13.0	185.4	149.7	296.9	291.3	290.3
0728_006	10.0		21.6	2.1	1.02	1.11	29.4	40.4	22.0	24.1	184.3	144.0	300.8	296.4	293.7
0728_007	10.0		15.3	1.5	0.95	1.05	29.4	44.6	30.5	34.0	181.9	137.3	300.6	296.2	293.5
0728_008	10.0		11.5	1.1	1.06	1.15	29.4	49.6	40.4	45.2	186.1	136.5	301.4	294.7	293.6
0728_010	10.0		11.5	1.1	1.11	1.21	29.4	50.8	42.9	45.4	188.3	137.5	304.3	296.9	296.2
0728_009	10.0		11.2	1.1	1.11	1.21	29.4	50.9	43.1	46.4	188.2	137.3	304.4	296.9	296.1
0728_011	15.0		120.8	11.9	1.06	1.05	29.4	32.9	7.2	6.1	455.2	422.3	325.3	322.1	326.4
0728_012	15.0		101.5	10.0	1.01	1.03	29.4	33.3	7.8	7.2	454.5	421.2	331.7	327.1	328.9
0728_013	15.0		81.3	8.0	1.07	1.11	29.4	34.3	9.8	9.0	457.7	423.5	343.2	335.4	335.4
0728_014	15.0		60.3	5.9	1.02	1.09	29.4	35.7	12.6	12.1	456.9	421.2	344.7	338.3	336.8
0728_015	15.0		40.0	3.9	0.89	0.98	29.4	38.4	18.1	18.3	451.9	413.5	343.2	337.3	335.4
0728_020	15.0		27.2	2.7	1.04	1.13	29.4	44.9	31.2	26.8	458.5	413.4	346.5	335.8	336.0
0728_016	15.0		26.2	2.6	1.01	1.10	29.4	45.0	31.4	27.9	457.3	412.3	345.2	334.0	333.5
0728_019	15.0		25.0	2.5	1.04	1.13	29.4	45.0	31.3	29.3	458.3	413.3	345.2	335.3	335.4
0728_018	15.0	4.5	22.4	2.2	1.03	1.12	29.4	45.0	31.2	32.6	458.1	413.1	600.0	600.0	600.0
0808_017	20.0		120.7	11.9	1.00	1.02	29.4	33.7	8.7	7.8	454.0	420.3	400.0	389.5	390.3
0804_001	20.0		120.4	11.9	1.03	1.04	29.4	33.3	7.8	7.8	454.9	421.6	387.8	382.2	385.6
0808_016	20.0		100.9	9.9	1.02	1.07	29.4	34.3	9.8	9.3	182.7	148.5	405.6	394.7	395.4
0808_015	20.0		80.1	7.9	1.00	1.08	29.4	35.5	12.2	11.7	183.1	147.6	408.8	398.1	398.2
0808_014	20.0		59.2	5.8	1.00	1.09	29.4	37.4	16.1	15.8	183.8	146.4	409.9	399.0	399.3
0804_002	20.0		40.2	4.0	0.96	1.06	29.4	40.8	22.8	23.3	182.5	141.7	398.5	384.7	384.3
0804_004	20.0	8.3	35.4	3.5	0.96	1.07	29.4	42.3	26.0	26.4	182.7	140.4	600.0	600.0	600.0
0804_005	20.0	8.6	35.4	3.5	0.96	1.07	29.4	42.3	25.9	26.4	182.7	140.3	600.0	600.0	600.0
0804_003	20.0	5.0	30.0	3.0	0.96	1.06	29.4	42.8	26.8	31.2	182.4	139.7	600.0	600.0	600.0

Table 3-4 Experimental conditions and results of CHF test on the conventional swirl tube (2).

Data name	IHF	$T_{burnout}$	V	Uax	Pin	Plocal	Tin	Tlocal	Dt_exp	Dt_wtr	Tsat	Tsub	TC-1	TC-2	TC-3
	[MW/m^2]	[sec]	[l/min]	[m/sec]	[MPa]	[MPa]	[°C]	[°C]	[°C]	[°C]	[°C]	[°C]	[°C]	[°C]	[°C]
0808_011	25.0		104.9	10.3	1.02	1.06	29.4	35.4	12.1	10.6	182.6	147.2	465.8	452.7	452.7
0808_012	25.0		80.1	7.9	1.00	1.07	29.4	37.3	15.9	13.9	183.1	145.7	468.6	452.0	450.5
0807_004	25.0		60.1	5.9	0.94	1.03	29.5	40.0	21.1	18.5	181.3	141.4	469.3	443.4	441.3
0807_003	25.0		59.9	5.9	0.94	1.03	29.4	40.0	21.3	18.6	181.2	141.2	470.5	443.3	441.0
0808_013	25.0		59.4	5.8	1.00	1.10	29.4	39.6	20.6	18.8	183.9	144.2	477.3	447.9	446.0
0807_005	25.0		56.0	5.5	0.98	1.08	29.4	40.6	22.5	19.9	183.2	142.6	485.2	458.0	493.0
0807_007	25.0	4.3	52.1	5.1	0.86	1.00	29.4	40.7	22.6	21.4	179.8	139.2	600.0	600.0	600.0
0807_006	25.0	3.6	50.1	4.9	0.84	0.94	29.4	40.5	22.2	22.2	177.2	136.7	600.0	600.0	600.0
0808_001	30.0		120.5	11.9	1.00	1.02	29.4	35.4	12.0	11.0	180.9	145.5	490.5	477.5	478.4
0807_010	30.0		120.1	11.8	0.95	0.96	29.4	35.7	12.7	11.1	178.2	142.5	502.7	492.4	490.2
0807_011	30.0		80.7	8.0	0.94	1.01	29.4	38.4	18.0	16.5	180.3	142.0	517.5	503.3	543.2
0807_012	30.0		80.7	8.0	0.94	1.01	29.4	38.4	18.1	16.5	180.5	142.1	518.8	505.1	547.2
0808_004	30.0		79.0	7.8	1.06	1.13	29.4	38.2	17.8	16.8	185.4	147.1	519.6	495.9	493.4
0808_003	30.0		79.0	7.8	1.06	1.13	29.4	38.4	18.1	16.8	185.4	147.0		497.6	496.9
0808_002	30.0		78.9	7.8	1.06	1.13	29.4	37.9	17.1	16.9	185.4	147.5		480.5	477.8
0807_013	30.0	4.6	74.9	7.4	1.02	1.09	29.4	38.6	18.6	17.8	183.7	145.1	600.0	600.0	600.0
0808_005	30.0	4.8	73.9	7.3	1.05	1.13	29.4	39.0	19.3	18.0	185.4	146.4	600.0	600.0	600.0
0808_006	30.0	5.3	69.8	6.9	1.04	1.13	29.4	39.2	19.6	19.0	185.2	146.0	600.0	600.0	600.0
0808_007	35.0		120.6	11.9	1.05	1.07	29.4	36.2	13.7	12.3	182.9	146.7	560.1	545.0	539.1
0808_009	35.0		109.8	10.8	1.05	1.09	29.4	36.7	14.6	13.5	183.6	146.9	560.2	545.6	562.5
0808_010	35.0	5.7	104.9	10.3	1.03	1.07	29.4	37.3	15.9	14.2	455.8	418.5	600.0	600.0	600.0
0808_008	35.0	4.1	98.9	9.7	1.00	1.06	29.4	37.3	15.9	15.0	182.4	145.1	600.0	600.0	600.0

Table 3-5 Results of FEM analyses for annular swirl tube.

IHF	Uax	FEM results		WHF	ht	WHF/IHF
		TC	Twall			
MW/m^2	m/sec	[°C]	[°C]	MW/m^2	W/m^2/K	
10	2	317.4	231.4	12.80	7.38E+04	1.28
	4	305.3	222.6	11.78	6.59E+04	1.18
	6	274.8	193.6	11.20	7.26E+04	1.12
	8	249	167.3	11.49	8.82E+04	1.15
	10	231.6	149.4	11.69	1.03E+05	1.17
	12	218.9	136.4	13.36	1.31E+05	1.34
	14	209.1	126.3	11.98	1.30E+05	1.20
15	2	372.2	240.9	19.87	1.16E+05	1.32
	4	368.1	238	19.48	1.03E+05	1.30
	6	360.7	232.7	18.81	9.92E+04	1.25
	8	346.5	221.2	17.85	9.84E+04	1.19
	10	325.1	200.3	17.68	1.09E+05	1.18
	12	307.1	181.9	17.91	1.23E+05	1.19
	14	293.3	167.7	18.08	1.37E+05	1.21
20	2	424.3	247.8	26.79	1.62E+05	1.34
	4	421.9	245.9	26.67	1.41E+05	1.33
	6	417.9	242.9	26.29	1.35E+05	1.31
	8	412.4	238.9	24.54	1.25E+05	1.23
	10	404.3	232.8	25.15	1.31E+05	1.26
	12	392	222.5	24.34	1.32E+05	1.22
	14	376.1	207	24.24	1.43E+05	1.21

IHF	Uax	FEM results		WHF	ht	WHF/IHF
		TC	Twall			
MW/m^2	m/sec	[°C]	[°C]	MW/m^2	W/m^2/K	
25	2	475.3	253.3	33.86	2.07E+05	1.35
	4	473.3	251.8	33.55	1.75E+05	1.34
	6	471.2	250.6	33.34	1.66E+05	1.33
	8	468.1	248.1	33.11	1.63E+05	1.32
	10	463.8	244.9	32.70	1.61E+05	1.31
	12	458	240.7	32.24	1.61E+05	1.29
	14	449.8	234.4	31.40	1.60E+05	1.26
30	2	525.6	258	40.65	2.59E+05	1.35
	4	524.7	257.4	40.73	2.12E+05	1.36
	6	522.8	256	40.43	2.00E+05	1.35
	8	520.7	254.6	40.09	1.94E+05	1.34
	10	518	252.6	40.06	1.92E+05	1.34
	12	514.5	249.9	39.63	1.91E+05	1.32
	14	510	246.6	39.22	1.90E+05	1.31
35	6	573.9	261	47.55	2.33E+05	1.36
	8	572.3	259.7	47.30	2.25E+05	1.35
	10	570.3	258.3	46.99	2.21E+05	1.34
	12	567.8	256.6	47.00	2.20E+05	1.34
	14	564.8	254.3	46.63	2.19E+05	1.33

Table 3-6 Results of FEM analyses for conventional tube.

IHF	Uax	FEM results		WHF	ht	WHF/IHF
		TC	Twall			
MW/m^2	m/sec	[°C]	[°C]	MW/m^2	W/m^2/K	
10	2	319	232.5	12.89	6.80E+04	1.29
	4	313.9	229.1	12.45	6.46E+04	1.24
	6	302.9	220.9	11.52	6.17E+04	1.15
	8	280.2	199.4	11.05	6.65E+04	1.11
	10	258.8	177.5	11.27	7.78E+04	1.13
	12	243.5	161.8	11.47	8.85E+04	1.15
	14	231.6	149.6	11.63	9.87E+04	1.16
15	2	367.6	240.6	19.21	9.97E+04	1.28
	4	365.2	239	19.00	9.50E+04	1.27
	6	361.6	236.4	18.62	9.29E+04	1.24
	8	356.1	232.6	18.16	9.17E+04	1.21
	10	347.1	225.6	17.43	9.08E+04	1.16
	12	333	212.8	16.92	9.41E+04	1.13
	14	317	196.7	16.99	1.04E+05	1.13
20	2	414.3	246.7	25.46	1.32E+05	1.27
	4	413	245.9	25.33	1.24E+05	1.27
	6	411	244.5	25.20	1.22E+05	1.26
	8	408.2	242.5	24.92	1.21E+05	1.25
	10	404.5	239.8	24.48	1.19E+05	1.22
	12	399.4	236.1	24.02	1.19E+05	1.20
	14	392.3	230.6	23.48	1.19E+05	1.17

IHF	Uax	FEM results		WHF	ht	WHF/IHF
		TC	Twall			
MW/m^2	m/sec	[°C]	[°C]	MW/m^2	W/m^2/K	
25	2	475.5	253.6	33.84	1.72E+05	1.35
	4	474.7	253	33.70	1.61E+05	1.35
	6	473.5	252.2	33.57	1.58E+05	1.34
	8	472	251	33.51	1.56E+05	1.34
	10	469.6	249.1	33.42	1.56E+05	1.34
	12	466.9	247	33.10	1.56E+05	1.32
	14	463.8	244.7	32.78	1.56E+05	1.31
30	2	529.9	262.2	40.72	2.04E+05	1.36
	4	525.4	258	40.68	1.92E+05	1.36
	6	524.6	257.4	40.85	1.89E+05	1.36
	8	522.9	255.9	40.59	1.86E+05	1.35
	10	521.3	254.8	40.38	1.85E+05	1.35
	12	519.7	253.7	40.00	1.83E+05	1.33
	14	518	252.7	39.71	1.82E+05	1.32
35	2	580.5	266.8	47.76	2.39E+05	1.36
	4	575.9	262.4	47.64	2.23E+05	1.36
	6	574.7	261.4	47.78	2.18E+05	1.37
	8	573.6	260.6	47.49	2.14E+05	1.36
	10	572.8	260.2	47.14	2.12E+05	1.35
	12	571.9	259.5	47.42	2.12E+05	1.35
	14	570.3	258.3	47.27	2.12E+05	1.35

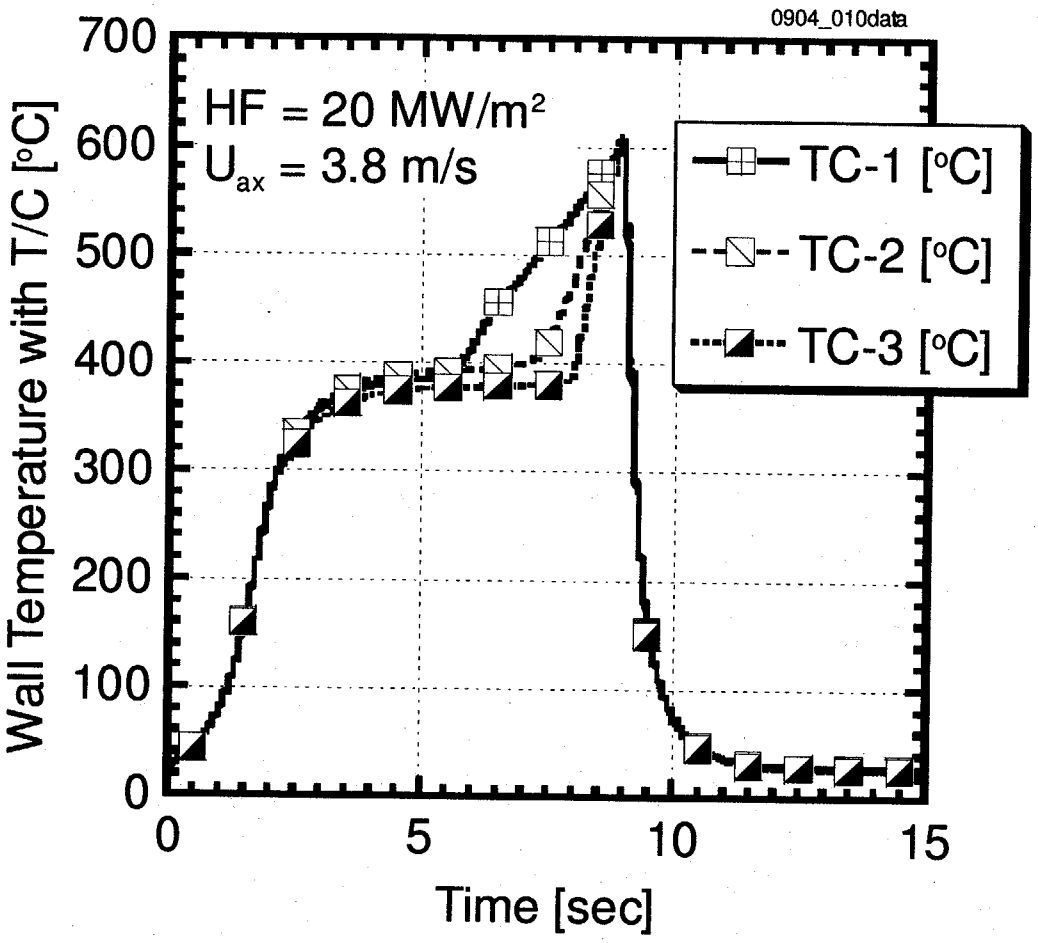

Figure 3-8 Typical temperature response at the burnout (Heat flux = 20 MW/m^2, Axial velocity, U_{ax} = 3.8 m/sec).

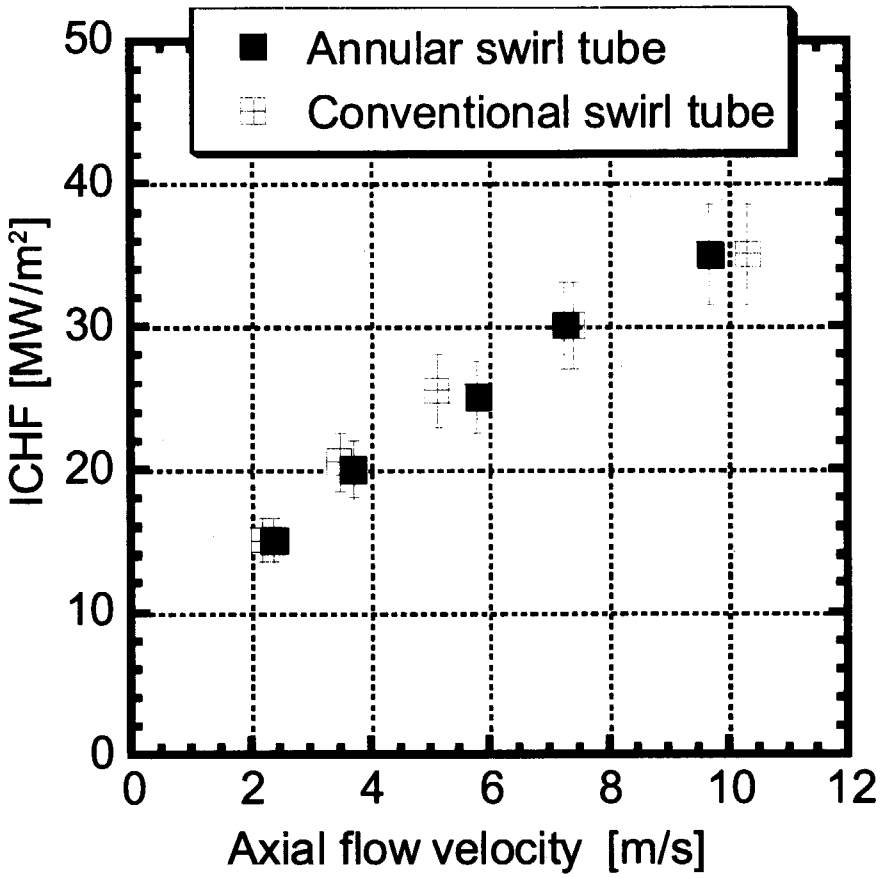

Figure 3-9 ICHF for annular swirl tube with twisted fins in comparison with conventional swirl tube.

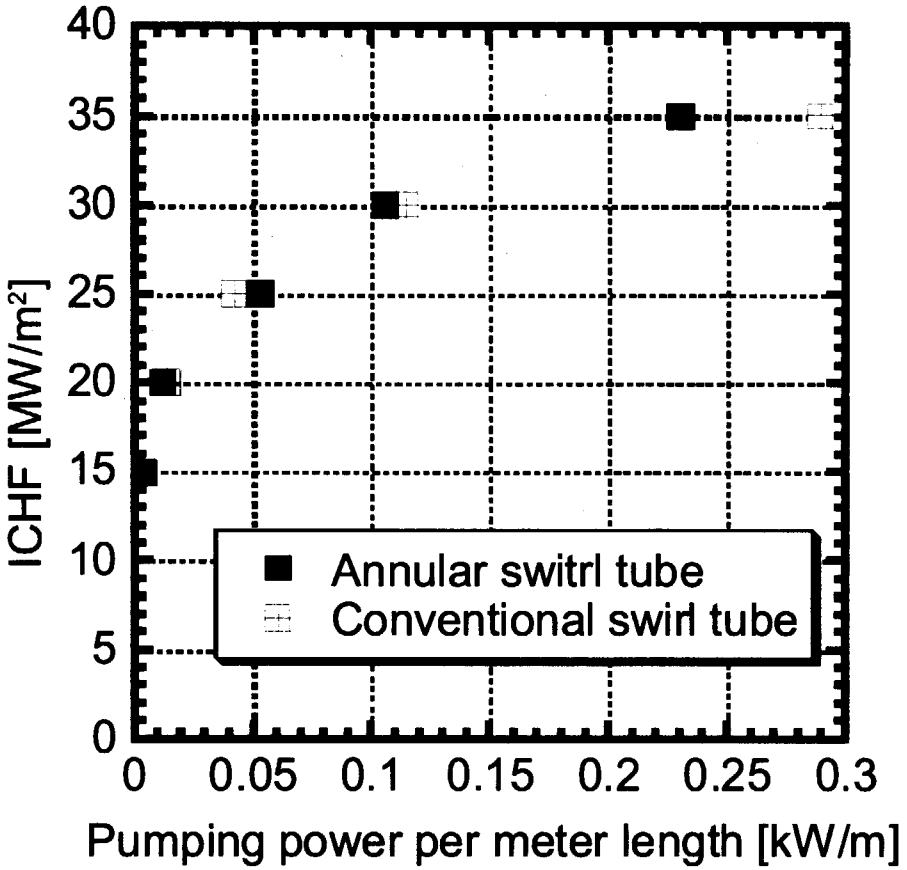

Figure 3-10 ICHF of test samples on pumping power.

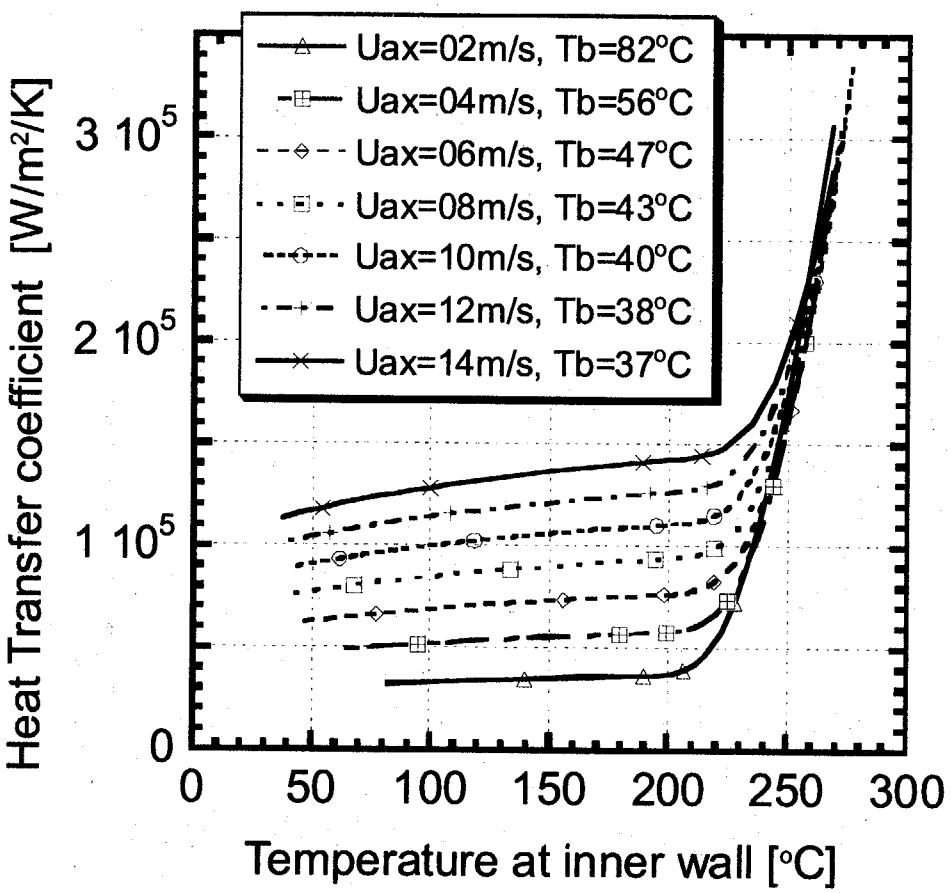

Figure 3-11 Typical heat transfer coefficients at several axial flow velocities.

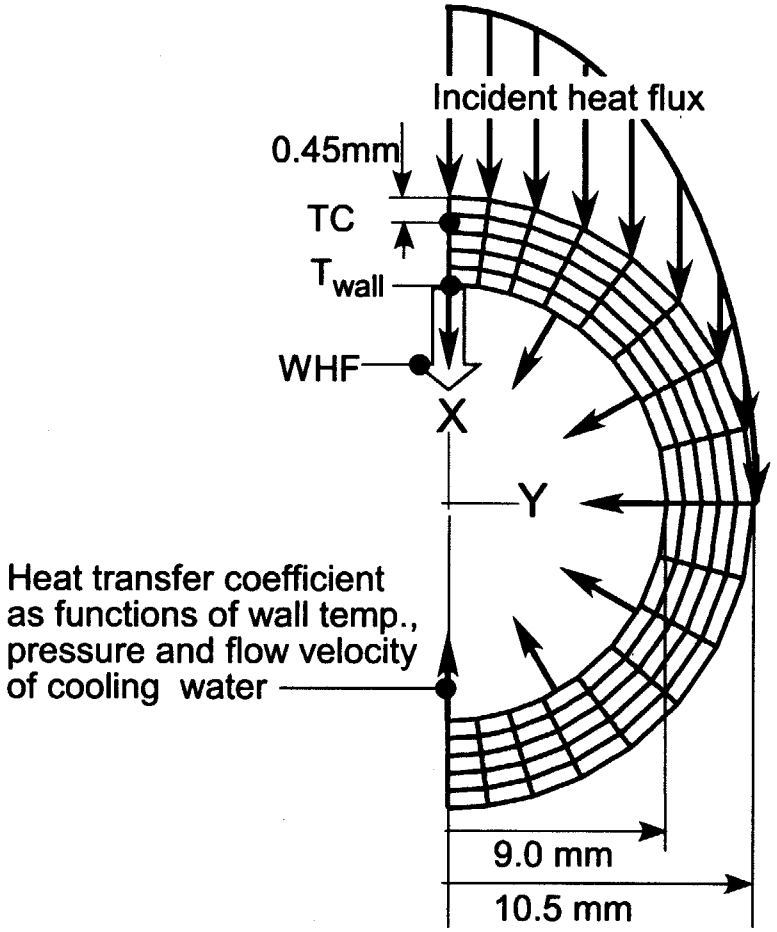

Figure 3-12 Finite element model and boundary conditions for heat conduction analyses of annular swirl tube and conventional swirl tube.

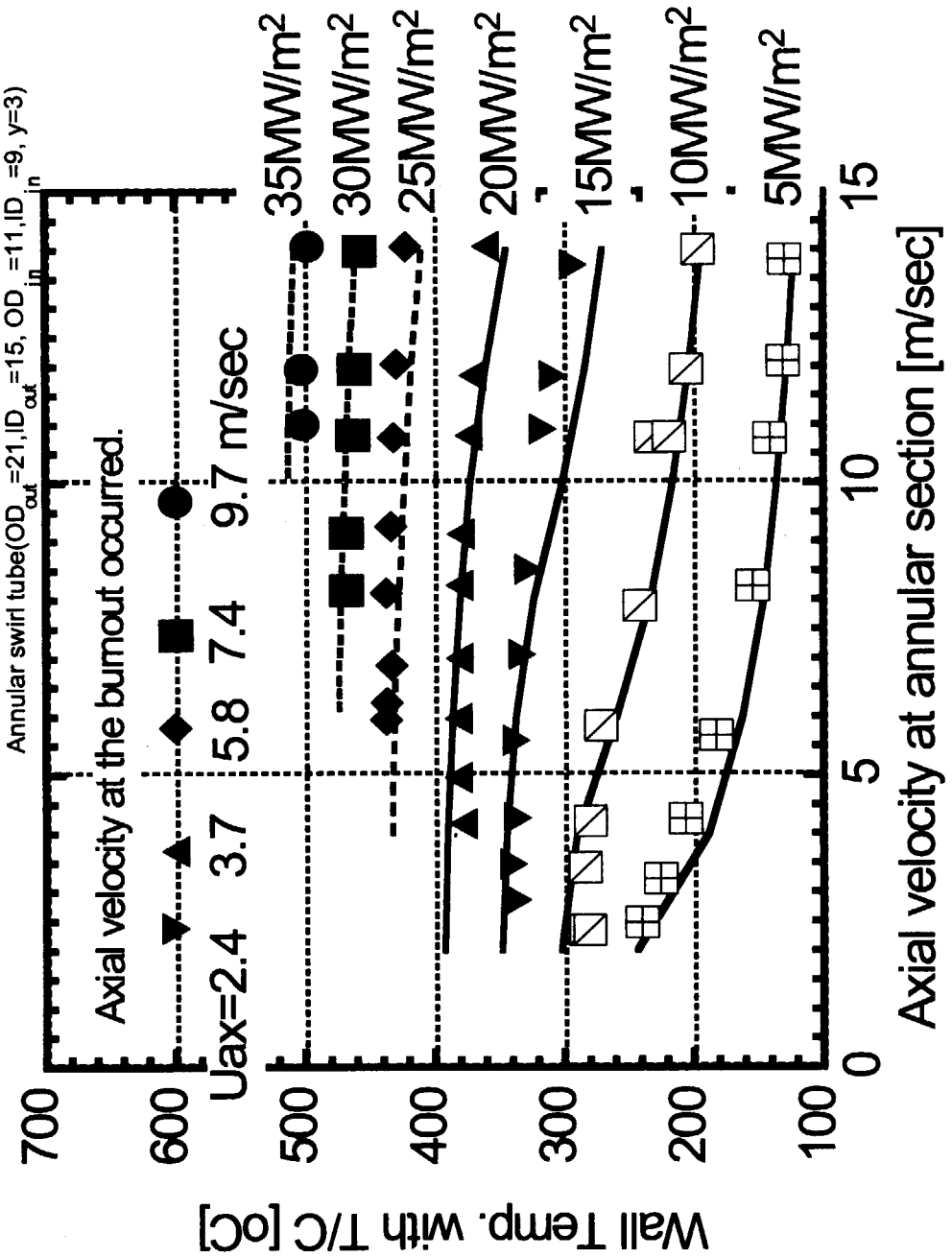

Figure 3-13 Comparisons of experimental wall temperatures with predicted values for annular swirl tube.

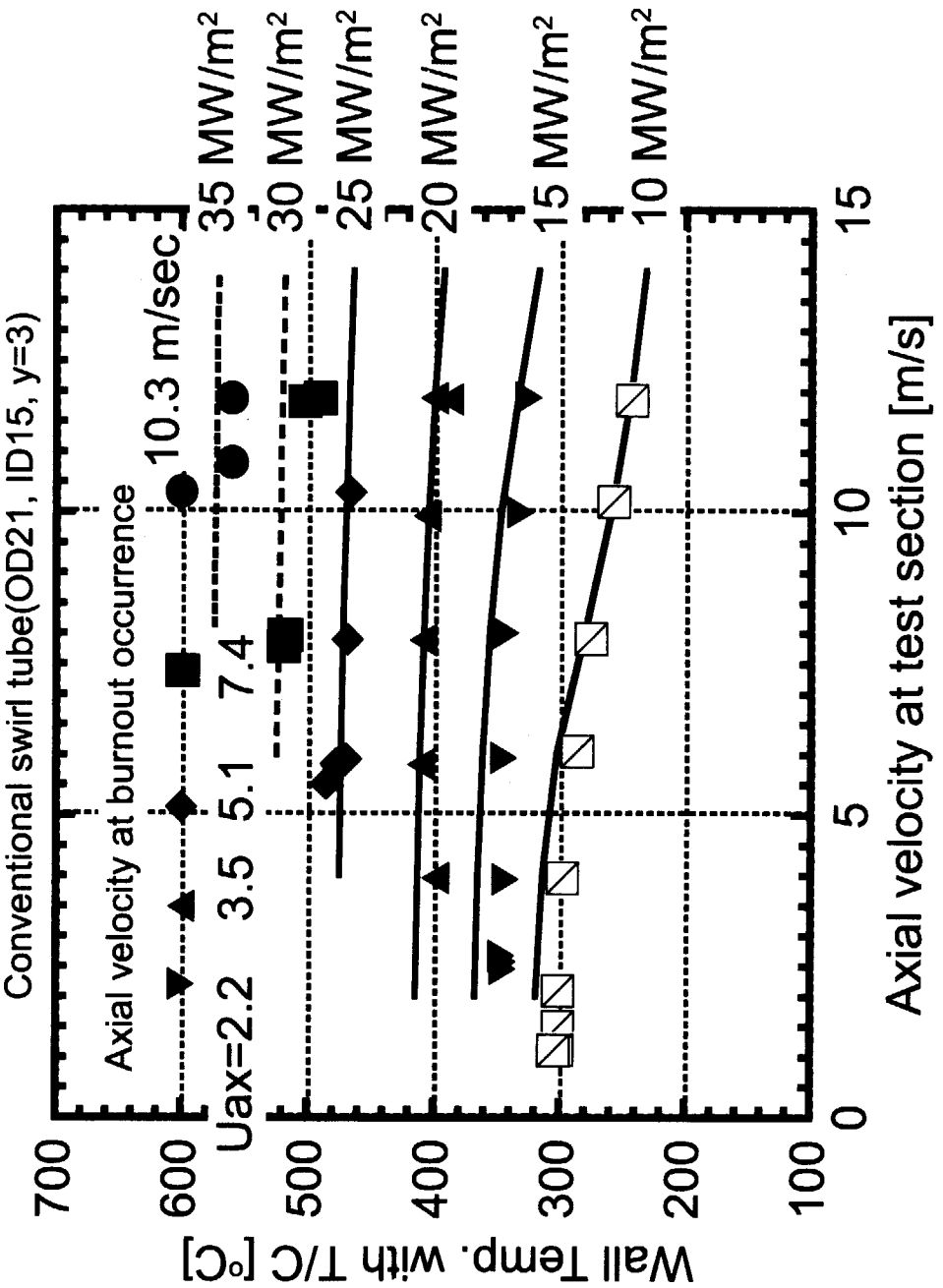

Figure 3-14 Comparisons of experimental wall temperatures with predicted values for conventional swirl tube.

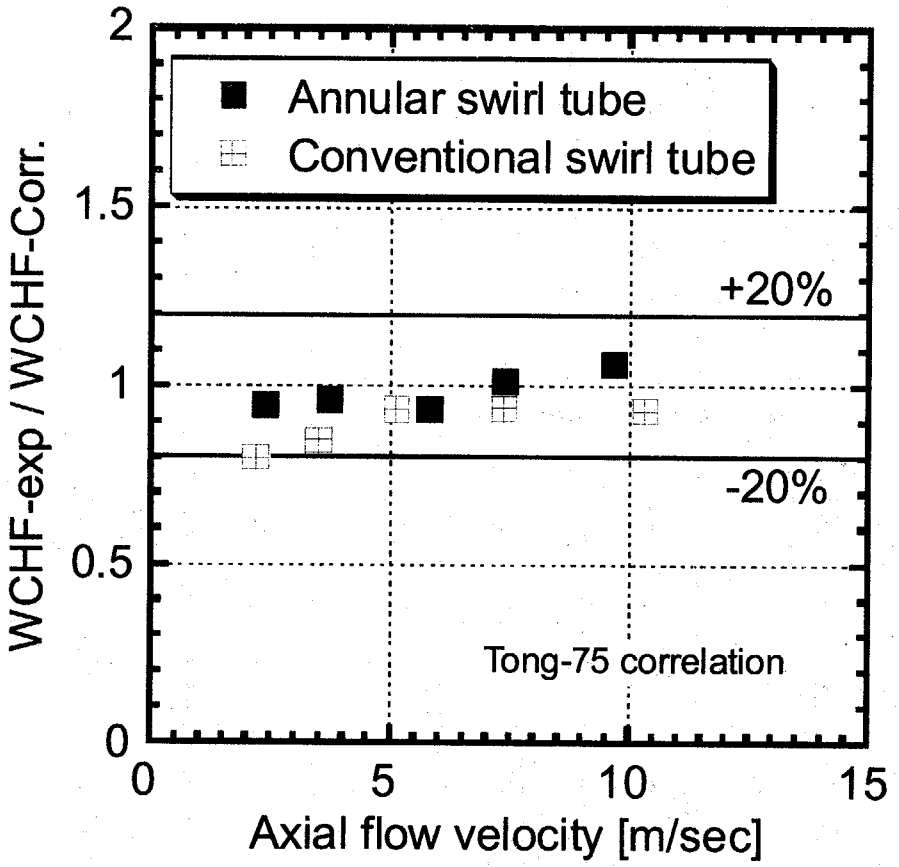

Figure 3-15 WCHF comparison between experiments and estimation by Tong-75 correlation as a function of axial flow velocity.

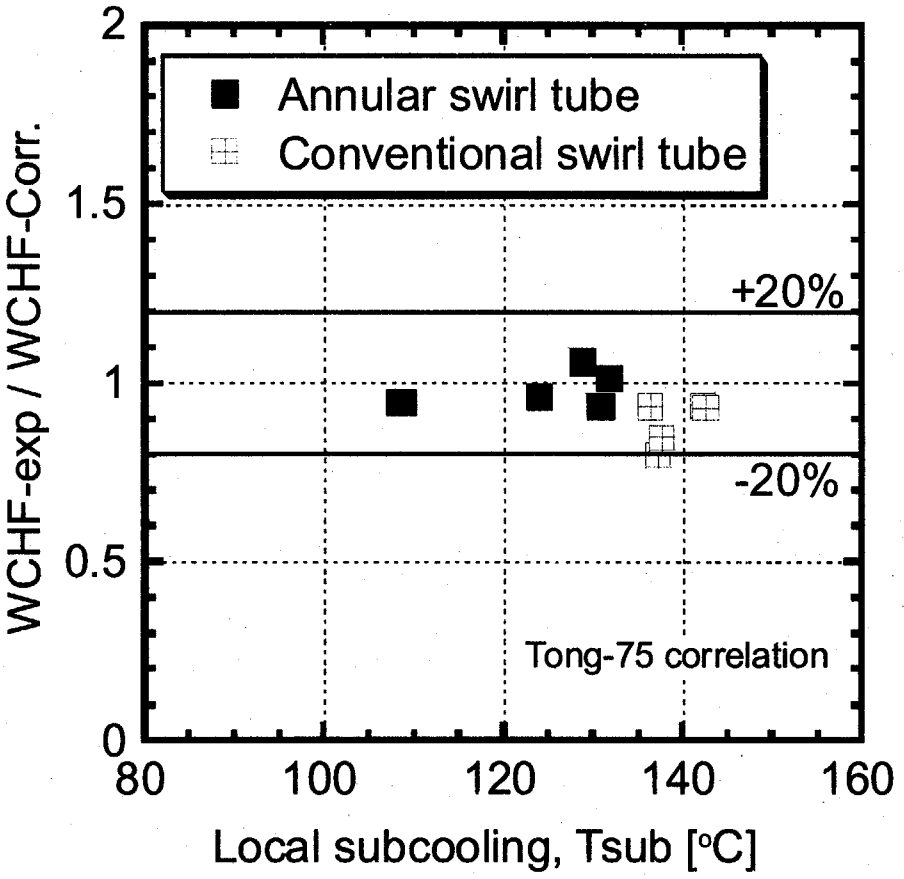

Figure 3-16 WCHF comparison between experiments and estimation by Tong-75 correlation as a function of local subcooling, $S_{tub}=T_{sat}-L_{ocal}$.

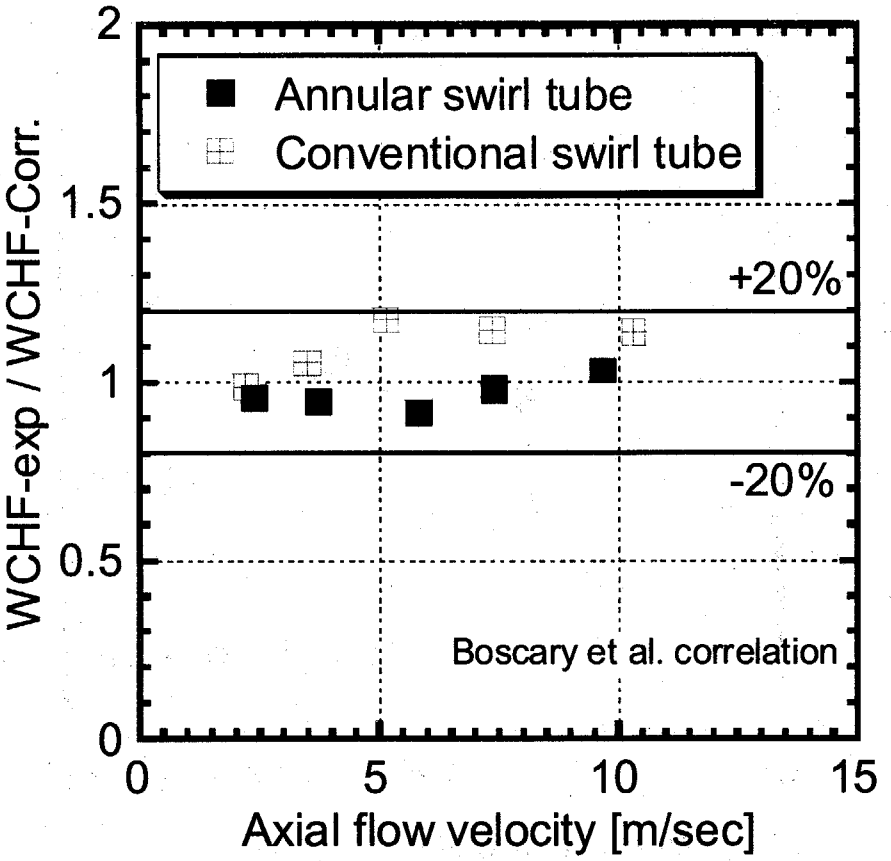

Figure 3-17 WCHF comparison between experiments and estimation by Boscary et al. correlation as a function of axial flow velocity.

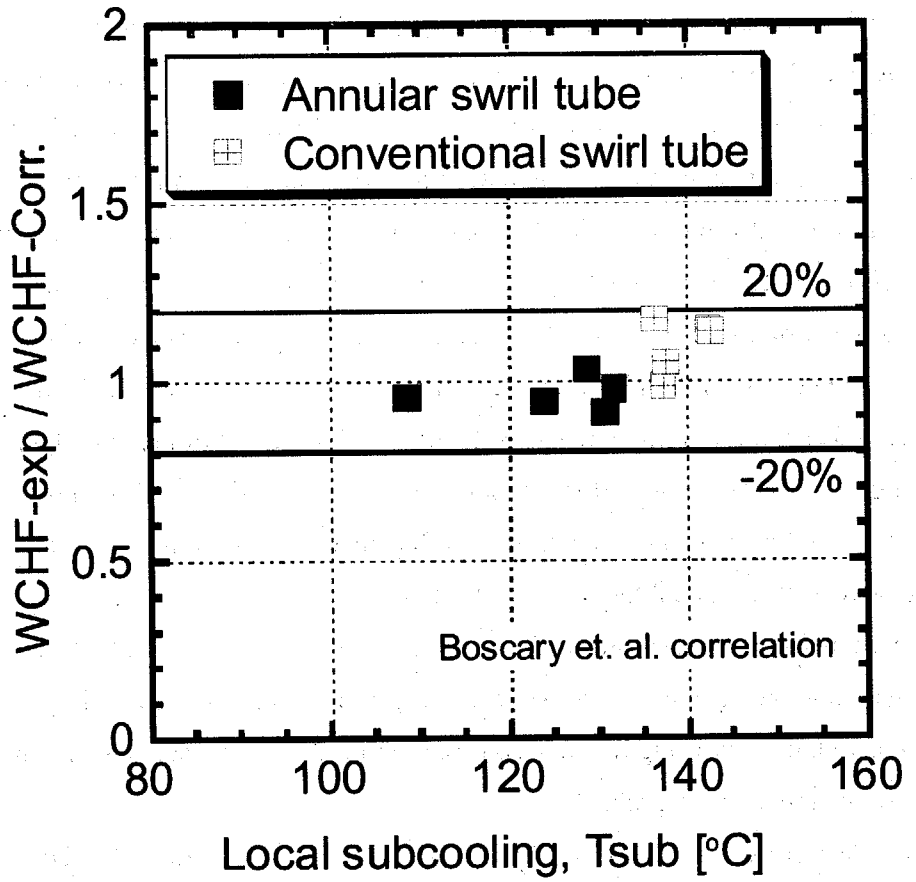

Figure 3-18 WCHF comparison between experiments and estimation by Boscary et al. correlation as a function of local subcooling, $S_{tub}=T_{sat}-L_{ocal}$.

4. Concluding remarks

Thermal hydraulic experiments measuring pressure drop and critical heat flux, CHF, of the annular swirl tube are performed to examine its applicability to the ITER divertor cooling structure. This annular tube consists of two concentric circular tubes, the outer tube and the inner tube. The outer tube with outer and inner diameters (OD and ID) of 21mm and 15mm is made of Cu-alloy, which is CuCrZr and one of candidate materials of the ITER divertor cooling tube. The inner tube with OD of 11 mm and ID of 9 mm is made of stainless steal. Its external surface has the twisted fins with twist ratio (y) of three to enhance its heat transfer performance. In the present study, the twist ratio is defined as a ratio of pitch of 180° rotation of the fin to ID of the outer tube. In this cooling tube, cooling water flows inside the inner tube first; the flow direction is changed at the end of tube, and then returns in the annulus between the outer and inner tubes with a swirl flow to cool the heated outer tube.

The friction factor correlation for the annular section with the twisted fins is made for the hydraulic designing of the vertical target. The least pressure drop at the end-return is obtained by using the hemispherical end-return. Its radius is the same as that of ID of the outer cooling tube.

The incident critical heat flux (ICHF) testing show no degradation of ICHF of the annular swirl tube in comparison with the conventional swirl tube whose dimensions are the same as those of the outer tube of the annular tube. A minimum axial velocity of 7.1 m/sec is required for 28 MW/m^2, which is the ITER design value. Applicability of both correlations of the heat transfer and the wall critical heat flux to the annular swirl tube is also examined by comparing the experimental results with those of the numerical analyses. It is found that the heat removal performance of the annular swirl tube can be estimated by these correlations.

These results show that thermal-hydraulic performance of the annular swirl tube is promising in application to the cooling structure for the ITER vertical target.

Acknowledgements

The authors would like to express their gratitude to Dr. T. Imai and the member of Plasma heating laboratory for their valuable discussions and support for carrying out

experiments in PBEF. They would acknowledge Dr. S. Matsuda, Dr. M. Seki, and Dr. Y. Okumura for their support and encouragements.

References

[1] R. Tivey, et al., ìITER divertor, design issues and research and development,î Fusion Engineering and Design 46 (1999) 207-220.

[2] A.R. Raffray, et al. ìCritical heat flux analysis and R&D for the design of the ITER divertor,î Fusion Engineering and Design, 45 (1999) 377-407.

[3] Escourbiac, Schlosser ñ Brief review about CHF tests on CEA 47 mock-up (AF1/ST2), P/CO 96 - 004, Cadarache, April 5, 1996.

[4] J. Schlosser, Completion of critical heat flux and thermal hydraulic testing of swirl tubes for ITER high heat flux components, NT/CO/98011, 23/4/98.

[5] R.M. Manglik and A.E. Bergles, îHeat transfer and pressure drop correlations for twisted-tape inserts in isothermal tube: Part II ñ transition and turbulent flows,î J. of Heat transfer, vol. 115 (1993) 890-896.

[6] M. Araki, M. Ogawa, T. Kunugi, K. Satoh, and S. Suzuki, ìExperimental on Heat Transfer of Smooth and Swirl Tubes under One-sided Heating conditions,î Int. J. Heat and Mass Transfer, **39**(1996) 3045-3055.

[7] Hibbit, Karlson and Sorenson Inc., ìABAQUS userís manual 5.8,î Providence, RI, USA, 1996.

[8] W.R. Gambil, R.D. Bundy, and R.W. Wansbrough, ìHeat Transfer, Burnout and Pressure Drop for Water in Swirl Flow Through Tubes with Internal Twisted Tapes,î ORNL-2911, Oakridge National Laboratory, 1960.

[9] L.S. Tong, ìA phenomenological study of critical heat flux,î ASME paper, 75-HT-68.

[10] J. Boscary, M. Araki, J. Schlosser, M. Akiba and F. Escourbiac, ìDimensional analysis of critical heat flux subcooled water flow under one-sided heating conditions for fusion application,î Fusion Engineering and Design, 43 (1998) 147-171.

This is a blank page.

国際単位系（SI）と換算表

表1　SI基本単位および補助単位

量	名称	記号
長さ	メートル	m
質量	キログラム	kg
時間	秒	s
電流	アンペア	A
熱力学温度	ケルビン	K
物質量	モル	mol
光度	カンデラ	cd
平面角	ラジアン	rad
立体角	ステラジアン	sr

表2　SIと併用される単位

名称	記号
分，時，日	min，h，d
度，分，秒	°，′，″
リットル	l，L
トン	t
電子ボルト	eV
原子質量単位	u

1 eV=1.60218×10^{-19}J

1 u=1.66054×10^{-27}kg

表3　固有の名称をもつSI組立単位

量	名称	記号	他のSI単位による表現
周波数	ヘルツ	Hz	s^{-1}
力	ニュートン	N	$m\cdot kg/s^2$
圧力，応力	パスカル	Pa	N/m^2
エネルギー,仕事,熱量	ジュール	J	N·m
工率，放射束	ワット	W	J/s
電気量，電荷	クーロン	C	A·s
電位，電圧，起電力	ボルト	V	W/A
静電容量	ファラド	F	C/V
電気抵抗	オーム	Ω	V/A
コンダクタンス	ジーメンス	S	A/V
磁束	ウェーバ	Wb	V·s
磁束密度	テスラ	T	Wb/m^2
インダクタンス	ヘンリー	H	Wb/A
セルシウス温度	セルシウス度	℃	
光束	ルーメン	lm	cd·sr
照度	ルクス	lx	lm/m^2
放射能	ベクレル	Bq	s^{-1}
吸収線量	グレイ	Gy	J/kg
線量等量	シーベルト	Sv	J/kg

表4　SIと共に暫定的に維持される単位

名称	記号
オングストローム	Å
バーン	b
バール	bar
ガル	Gal
キュリー	Ci
レントゲン	R
ラド	rad
レム	rem

1 Å=0.1nm=10^{-10}m

1 b=100fm^2=10^{-28}m^2

1 bar=0.1MPa=10^5Pa

1 Gal=1cm/s^2=10^{-2}m/s^2

1 Ci=3.7×10^{10}Bq

1 R=2.58×10^{-4}C/kg

1 rad=1cGy=10^{-2}Gy

1 rem=1cSv=10^{-2}Sv

表5　SI接頭語

倍数	接頭語	記号
10^{18}	エクサ	E
10^{15}	ペタ	P
10^{12}	テラ	T
10^{9}	ギガ	G
10^{6}	メガ	M
10^{3}	キロ	k
10^{2}	ヘクト	h
10^{1}	デカ	da
10^{-1}	デシ	d
10^{-2}	センチ	c
10^{-3}	ミリ	m
10^{-6}	マイクロ	μ
10^{-9}	ナノ	n
10^{-12}	ピコ	p
10^{-15}	フェムト	f
10^{-18}	アト	a

（注）

1．表1－5は「国際単位系」第5版，国際度量衡局1985年刊行による。ただし,1 eVおよび1 uの値はCODATAの1986年推奨値によった。

2．表4には海里，ノット，アール，ヘクタールも含まれているが日常の単位なのでここでは省略した。

3．barは，JISでは流体の圧力を表わす場合に限り表2のカテゴリーに分類されている。

4．EC閣僚理事会指令ではbar，barnおよび「血圧の単位」mmHgを表2のカテゴリーに入れている。

換算表

力	N(=10^5dyn)	kgf	lbf
	1	0.101972	0.224809
	9.80665	1	2.20462
	4.44822	0.453592	1

粘度　1 Pa·s(N·s/m^2)=10 P(ポアズ)(g/(cm·s))

動粘度　1m^2/s=10^4St(ストークス)(cm^2/s)

圧力	MPa(=10bar)	kgf/cm^2	atm	mmHg(Torr)	lbf/in^2(psi)
	1	10.1972	9.86923	7.50062×10^3	145.038
	0.0980665	1	0.967841	735.559	14.2233
	0.101325	1.03323	1	760	14.6959
	1.33322×10^{-4}	1.35951×10^{-3}	1.31579×10^{-3}	1	1.93368×10^{-2}
	6.89476×10^{-3}	7.03070×10^{-2}	6.80460×10^{-2}	51.7149	1

エネルギー・仕事・熱量	J(=10^7 erg)	kgf·m	kW·h	cal(計量法)	Btu	ft·lbf	eV
	1	0.101972	2.77778×10^{-7}	0.238889	9.47813×10^{-4}	0.737562	6.24150×10^{18}
	9.80665	1	2.72407×10^{-6}	2.34270	9.29487×10^{-3}	7.23301	6.12082×10^{19}
	3.6×10^6	3.67098×10^5	1	8.59999×10^5	3412.13	2.65522×10^6	2.24694×10^{25}
	4.18605	0.426858	1.16279×10^{-6}	1	3.96759×10^{-3}	3.08747	2.61272×10^{19}
	1055.06	107.586	2.93072×10^{-4}	252.042	1	778.172	6.58515×10^{21}
	1.35582	0.138255	3.76616×10^{-7}	0.323890	1.28506×10^{-3}	1	8.46233×10^{18}
	1.60218×10^{-19}	1.63377×10^{-20}	4.45050×10^{-26}	3.82743×10^{-20}	1.51857×10^{-22}	1.18171×10^{-19}	1

1 cal= 4.18605J（計量法）

= 4.184J（熱化学）

= 4.1855J（15℃）

= 4.1868J（国際蒸気表）

仕事率　1 PS(仏馬力)

= 75 kgf·m/s

= 735.499W

放射能	Bq	Ci
	1	2.70270×10^{-11}
	3.7×10^{10}	1

吸収線量	Gy	rad
	1	100
	0.01	1

照射線量	C/kg	R
	1	3876
	2.58×10^{-4}	1

線量当量	Sv	rem
	1	100
	0.01	1

（86年12月26日現在）

Quantitative Experiments on Thermal Hydraulic Characteristics of an Annular Tube with Twisted Fins